NATIONAL ADVISORY COMMITTEE FOR AERONAUTICS

TECHNICAL NOTE 3760

AERODYNAMIC MIXING DOWNSTREAM FROM LINE SOURCE OF

HEAT IN HIGH-INTENSITY SOUND FIELD

By William R. Mickelsen and Lionel V. Baldwin

Lewis Flight Propulsion Laboratory
Cleveland, Ohio

NACA

Washington
August 1956

ERRATA

NACA Technical Note 3760

By William R. Mickelsen and Lionel V. Baldwin
August 1956

Page 7: Replace with attached page.

Equation (14) page 8: Change

$$\left(2\pi f\tau + \frac{\pi f x}{U}\right) \text{ to } \left(2\pi f\tau - \frac{\pi f x}{U}\right)$$

Equation (17) pages 10 and 25: Change

$$2\pi f\tau + \pi f t \text{ to } 2\pi f\tau - \pi f t$$

Equations (25) page 12, (26) page 13, (28) page 13: Change

$$\left(2\pi f\tau + 2\pi f\,\frac{X}{U}\right) \text{ to } \left(2\pi f\tau - 2\pi f\,\frac{X}{U}\right)$$

Equations (25) page 12, (26) page 13, (27) page 13, (28) page 13, (29) pages 13 and 24, and (B23) page 38: Change

$$2\pi f\tau + \frac{\pi f X}{U} \text{ to } 2\pi f\tau - \frac{\pi f X}{U}$$

Equation (B6) page 34: Change the term in brackets to

$$\left[-\cos(2\pi f\tau) + \cos\left(2\pi f\tau - 2\pi f\,\frac{X}{U} - 2\beta\right) - \frac{2Y}{y_{max}}\right]^2$$

Equation (B7) page 34: Change the term in brackets to

$$\left[+\cos\left(2\pi f\tau - 2\pi f\,\frac{X}{U} - 2\beta\right)\right]^2$$

Equation (B11), page 35: The upper limit on the first integral should be

$$\pi f\,\frac{X}{U}\sqrt{\frac{U^2}{4\pi^2 f^2 \omega_X}\left(1 + \frac{2v^2}{U^2}\right)}$$

Equations (B14) page 36, (B15) page 36, (B21) page 37, and page 37, line 9: Change

$$2\pi f\tau + 2\pi f\,\frac{X}{U} \text{ to } 2\pi f\tau - 2\pi f\,\frac{X}{U}$$

Equation (B24) page 39: The limits should read

$$\int_{-\pi f \frac{X}{U}}^{2\pi - \pi f \frac{X}{U}}$$

Page 8, line 9: The term τ should be τ_o.

Page 36, line 4: Equation (12) should be equation (13).

Page 36, line 8: The variable should be $\varphi = 2\pi f \tau - 2\pi f \frac{X}{U} - \frac{\pi}{2}$

Equations (B36) page 41, (B37) page 41, and (B38) page 42: Change

$$2\pi f \tau_1 + \frac{2\pi f x_1}{U} \quad \text{to} \quad 2\pi f \tau_1 - \frac{2\pi f x_1}{U}$$

Equation (B34) page 41: Change

$$2\pi f \tau_1 + \frac{\pi f x}{U} \quad \text{to} \quad 2\pi f \tau_1 - \frac{\pi f x}{U}$$

Equation (B38) page 42: Change

$$2\pi f \tau_1 + \frac{\pi f x_1}{U} \quad \text{to} \quad 2\pi f \tau_1 - \frac{\pi f x_1}{U}$$

Page 39: Line 3 should read "where $\varkappa = 2\pi f \tau - \pi f \frac{X}{U}$

Figure 1, page 53: The values of $f\tau$, 0, 1/6, 2/6, 3/6, 4/6, and 5/6, should read, respectively 3/6, 2/6, 1/6, 0, 5/6, and 4/6.

Figure 4, page 58: The values of $f\tau$, 0, .05, .10, .15, .20, and .25, should be, respectively .50, .45, .40, .35, .30, and .25.

$$d = \frac{\sqrt{2}\sqrt{\overline{v^2}}}{2\pi f}\left[1 - \cos\left(2\pi f\tau\right)\right] \tag{11}$$

where the constant of integration has been evaluated by setting $d = 0$ at $\tau = 0$.

The position of the wake center at x for successive instants of the time τ may be derived from consideration of the following displacement sketch:
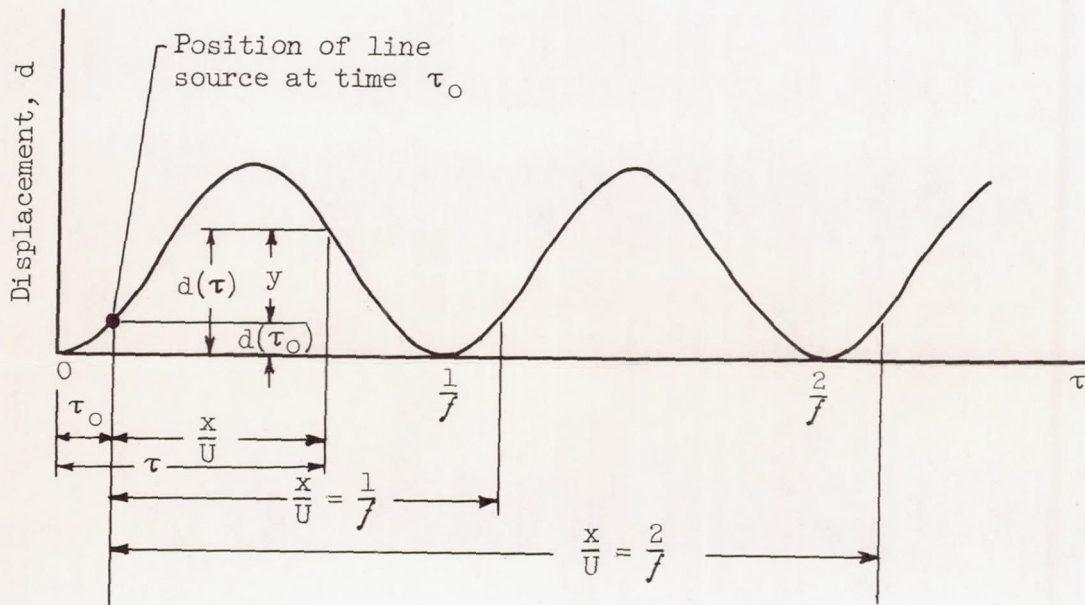
A line element released from the line source at time τ_0 reaches the axial station x after a residence time x/U. The lateral displacement y from the flow-axis plane is given by

$$y = d(\tau) - d(\tau_0) = d(\tau) - d\left(\tau - \frac{x}{U}\right) \tag{12}$$

where $d(\tau)$ is d evaluated at time τ and $d(\tau - x/U)$ is d at time $\tau - (x/U)$. By combining equation (11) with equation (12), the time history of the position of the center of the molecular-diffusion wake at any axial station x is

$$y = \frac{\sqrt{2}\sqrt{\overline{v^2}}}{2\pi f}\left\{\left[1 - \cos\left(2\pi f\tau\right)\right] - \left[1 - \cos\left(2\pi f\tau - 2\pi f\frac{x}{U}\right)\right]\right\} \tag{13}$$

TABLE OF CONTENTS

NATIONAL ADVISORY COMMITTEE FOR AERONAUTICS

———————

TECHNICAL NOTE 3760

———————

AERODYNAMIC MIXING DOWNSTREAM FROM LINE SOURCE OF

HEAT IN HIGH-INTENSITY SOUND FIELD

By William R. Mickelsen and Lionel V. Baldwin

SUMMARY

The processes of fuel-air preparation, combustion, and exhaust-gas mixing in jet-engine combustors depend to a large degree on aerodynamic mixing. Since combustors commonly have intense sound fields, it is of interest to investigate the effect of sound on the fundamental mixing process. This report describes a theoretical and experimental investigation of the aerodynamic mixing by a standing sound wave downstream from a continuous line source of heat.

By a kinematic analysis of the motion of the molecular-diffusion wake, equations are derived for the time variation of temperature and the time-mean temperature at points throughout the mixing region. The analysis shows that standing sound waves displace the diffusion wake in a manner similar to the displacements of a flag waving in a harmonic mode. The diffusion-wake displacement has nodal points downstream from the line source at distances which are integer multiples of the ratio (stream velocity)/(sound-wave frequency). The maximum wake displacement occurs at the antinodal distances and is equal to $(\sqrt{2} \times$ rms transverse velocity fluctuation)/($\pi \times$ sound-wave frequency). The theoretical analysis considers two general cases: (a) small and (b) large geometrical deformations of the diffusion wake by the transverse sound waves. The analysis shows that the deformations are characterized by stretching of the wake and by the relative magnitudes of the wake radius of curvature and thickness. The stretching is greater for high sound intensities. The curvature is greater for high sound intensities and high sound frequencies. When the wake suffers negligible deformation, the sound field contributes to the mixing in the time-mean sense; but the instantaneous, or local spatial, structure of the temperature field is unaffected. For the case of appreciable wake deformation, the temperature field is substantially changed in both the time-mean and instantaneous senses.

Experimental measurements confirmed the theoretical analysis for the case of negligible deformation of the diffusion wake, but no measurements were made for the case of appreciable deformation. The experiment was carried out in a low-turbulence airstream with superimposed transverse velocity fluctuations associated with a standing sound wave. The mixing region downstream from the line source of heat was at a pressure node of the standing sound wave so that pressure fluctuations were negligible. The amplitude of the transverse velocity fluctuations corresponded to a sound pressure level of 147 decibels, and the wave frequency was 104 cycles per second. Time-mean temperatures were measured with a thermopile probe. Instantaneous temperatures were measured by two different methods: resistance thermometry and hot-wire anemometry. The velocity fluctuations in the sound field were measured by hot-wire anemometry.

In order to facilitate application of the results to practical problems, a special section is included in which equations and methods are summarized.

INTRODUCTION

Aerodynamic mixing is an important factor in fuel-air preparation, combustion, and exhaust-gas mixing in jet-engine combustors. Because of its importance, it is of interest to investigate aerodynamic mixing under flow conditions commonly found in combustors. Although jet-engine combustors often have extremely intense sound fields, little attention has been given to the effect of sound-wave disturbances on aerodynamic mixing. The research described in this report covers a fundamental investigation of aerodynamic mixing in a low-turbulence airstream having a single-frequency, plane, transverse, standing sound wave.

Mixing in fluid streams proceeds locally by molecular motion (molecular diffusion) and on a larger scale by the turbulent velocity fluctuations, which transport fluid volumes composed of many molecules. It is reasonable to expect that the velocity fluctuations arising from the passage of sound pressure waves contribute to the mixing process in a manner somewhat similar to that of turbulence. The data in reference 1 show that the approach stream in a smooth-burning ram-jet combustor contained sound and turbulence velocity fluctuations of the same order of magnitude; the data of reference 2 show that screeching combustors have velocity fluctuations due to sound that may be several orders of magnitude larger than the turbulent velocity fluctuations.

Since the velocity fluctuations responsible for aerodynamic mixing are usually slow compared with the flow velocity through the combustor, the concentration of heat or mass in mixing regions fluctuates with time and varies irregularly from point to point in space. In turbulent mixing,

concentration fluctuations in time and space may also be due to the finite range of turbulent eddy sizes, since the smallest turbulent eddies are of a much larger scale than molecular mean free path. Experiments in turbulent mixing (refs. 3 and 4) have shown that concentration fluctuations can be of nearly as great a magnitude as the mean concentration at points throughout the mixing region. For these reasons, it is evident that mixing should be considered in the instantaneous sense as well as in the time-mean sense. Mixing in the instantaneous sense can be described by the time history of concentration fluctuations at a point in space, and mixing in the time-mean sense can be described by the long-time average of concentration at a point in space.

In order to investigate the fundamentals of the aerodynamic mixing due to sound, an experimental and theoretical study was made of the mixing downstream from a line source of heat in an intense sound field. The turbulence in the airstream was kept at a negligible level so that the mixing process was due only to the sound field and molecular diffusion. To prevent vortex shedding, the electrically heated wire that formed the line source had a small diameter. The center plane of the two-dimensional mixing region was placed at the velocity antinode and pressure node of a plane standing sound wave so that the sound pressure fluctuations were negligible and the sound disturbance velocities were transverse to the stream direction as shown in the following sketch:
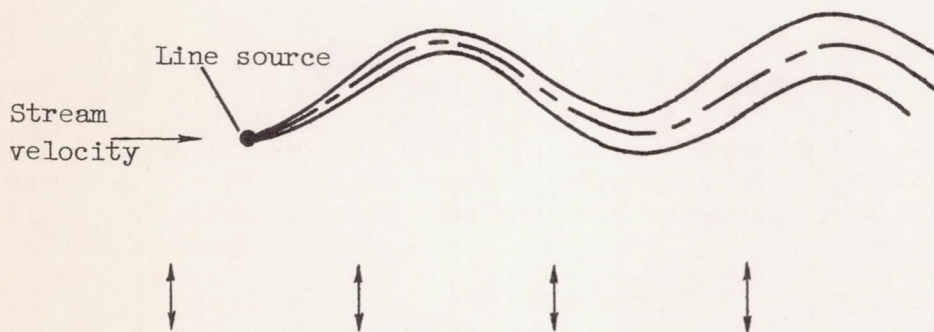
Transverse velocity fluctuations imposed by standing sound wave

The magnitude of the transverse velocity fluctuations corresponded to a sound field having a sound pressure level of 147 decibels. The transverse velocity fluctuation was nearly sinusoidal and had a frequency of 104 cycles per second. The instantaneous temperature was measured by a resistance thermometer and a hot-wire anemometer, and the transverse velocity fluctuations were measured by hot-wire anemometry. The time-mean temperatures were measured with a thermopile probe.

By a kinematic description of the mixing region, equations are de-
rived for the time variation of temperature and for the time-mean tem-
perature at points throughout the mixing region. This theoretical analysis
is made for two cases of interest: (a) negligible geometrical deforma-
tions of the diffusion wake by the sound field and (b) appreciable
deformations of the diffusion wake. For the case of negligible deforma-
tion of the diffusion wake, the theoretical analysis is compared with
measured values of the instantaneous and mean temperatures at various
points downstream from the line source of heat. By means of the theo-
retical analysis, a comparison is made between the cases of negligible
and appreciable wake deformation.

THEORETICAL ANALYSIS

The analysis of the temperature field in the mixing region is based
on a kinematic description of the displacement of a molecular-diffusion
wake by a transverse, plane, standing sound wave. A pictorial represen-
tation of the wake displacement is shown in figure 1(a). As shown in
the following analysis, the displacement of the wake is similar to the
displacement of a flag waving in a harmonic mode. The center of the
wake has a sinusoidal shape; and the molecular diffusion proceeds as
the wake elements pass downstream, as shown by the temperature profiles
in figure 1(a). From the kinematic analysis, expressions are derived
for the time variation of temperature and for the time-mean temperature
at fixed points throughout the mixing region.

Molecular-Diffusion Wake

The molecular diffusion of heat in a fluid stream at constant pres-
sure is described by the Fourier-Poisson equation (ref. 5) derived from
the Fourier-Biot heat-flux law. The Fourier-Poisson equation is

$$\frac{Dh}{Dt} = \frac{\partial}{\partial x_i}\left(\alpha\, \frac{\partial h}{\partial x_i}\right) \qquad (i = 1,2,3) \qquad (1)$$

where Dh/Dt is the total derivative of the volume specific enthalpy
h, which is defined by

$$h = \int_{T_{am}}^{T} \rho c_p\, dT \qquad (2)$$

and the coefficient of thermal diffusivity α is

$$\alpha = \frac{k}{\rho c_p} \tag{3}$$

(Symbols are defined in appendix A.)

For the case of molecular diffusion of mass, an equation similar to equation (1) can be derived from Fick's mass-flux law:

$$\frac{D\mathscr{C}}{Dt} = \frac{\partial}{\partial x_i}\left(D_M \frac{\partial \mathscr{C}}{\partial x_i}\right) \qquad (i = 1,2,3) \tag{4}$$

where D_M is the molecular-diffusion coefficient and $\mathscr{C}$ is the concentration of the diffusing gas. Since equations (1) and (4) are identical except for the coefficients α and D_M, their solutions for specific problems are also identical except for the coefficients. Because of the close similarity of equations (1) and (4), the following theoretical analysis applies in essence to the mixing of fluids with different heat contents or of different physical properties.

If the coefficient of thermal diffusivity is essentially constant, and if a molecular spreading coefficient ω is defined by

$$\omega = \int_0^t \alpha \, dt \tag{5}$$

then equation (1) may be written

$$\frac{Dh}{D\omega} = \frac{\partial^2 h}{\partial x_i^2} \qquad (i = 1,2,3) \tag{6}$$

If the fluid field is at rest, or if a coordinate system is used that moves along with the stream, then equation (6) can be written in terms of a Cartesian coordinate system (ξ, η, ζ):

$$\frac{\partial h}{\partial \omega} = \frac{\partial^2 h}{\partial \xi^2} + \frac{\partial^2 h}{\partial \eta^2} + \frac{\partial^2 h}{\partial \zeta^2} \tag{7}$$

As shown in reference 6, the solution of equation (7) for an instantaneous line source lying along the ζ-axis and emitted at $t = 0$ is given by

$$h = \frac{H/l}{4\pi\omega} e^{-\frac{\xi^2 + \eta^2}{4\omega}} \tag{8}$$

where H/l is the heat per unit length emitted at $t = 0$. Equation (8) is used in the subsequent derivation of an exact model for instantaneous temperature in the mixing region.

By assuming that diffusion in the stream direction is negligible, the following approximate equation for diffusion from a continuous line source in a stream flowing with velocity U in the x-direction is derived in reference 7:

$$h = \frac{q/l}{U\sqrt{4\pi\omega_x}} \cdot e^{-\frac{\eta^2}{4\omega}}$$ (9)

where η is the lateral distance from the molecular-wake center to a fixed point in space, q/l is the rate of heat release per unit length at the line source, and $\omega_x = \alpha X/U$. Equation (9) is used in the subsequent derivation of an approximate model for instantaneous temperature in the mixing region. The temperature difference $\Delta T = T - T_{am}$ can be determined from the volume specific enthalpy h by means of tables or graphs based on equation (2).

Kinematics of Molecular-Diffusion Wake in Transverse Sound Field

A kinematic description of the motion of the molecular-diffusion wake is necessary to subsequent derivations of the instantaneous and time-mean temperatures in the mixing region. This section describes the wake motion in terms of the time τ associated with the velocity fluctuations of the standing sound wave and of the distance x downstream from the line source of heat.

The transverse velocity fluctuation associated with the sound wave is assumed to have a sinusoidal form given by

$$v = \sqrt{2}\ \sqrt{\overline{v^2}}\ \sin\ (2\pi f \tau)$$ (10)

where $\sqrt{\overline{v^2}}$ is the root-mean-square value of the velocity wave form, f is the sound-wave frequency, and τ is time.

A fluid line element in the stream has a transverse motion caused by the velocity fluctuation v and a resulting transverse displacement d. The time history of the displacement d of a line element in the center of the molecular-diffusion wake is given by the integral of equation (10):

$$d = \frac{\sqrt{2}\sqrt{\overline{v^2}}}{2\pi f} \left[1 - \cos\left(2\pi f\tau\right)\right] \tag{11}$$

where the constant of integration has been evaluated by setting $v = 0$ at $\tau = 0$.

The position of the wake center at x for successive instants of the time τ may be derived from consideration of the following displacement sketch:
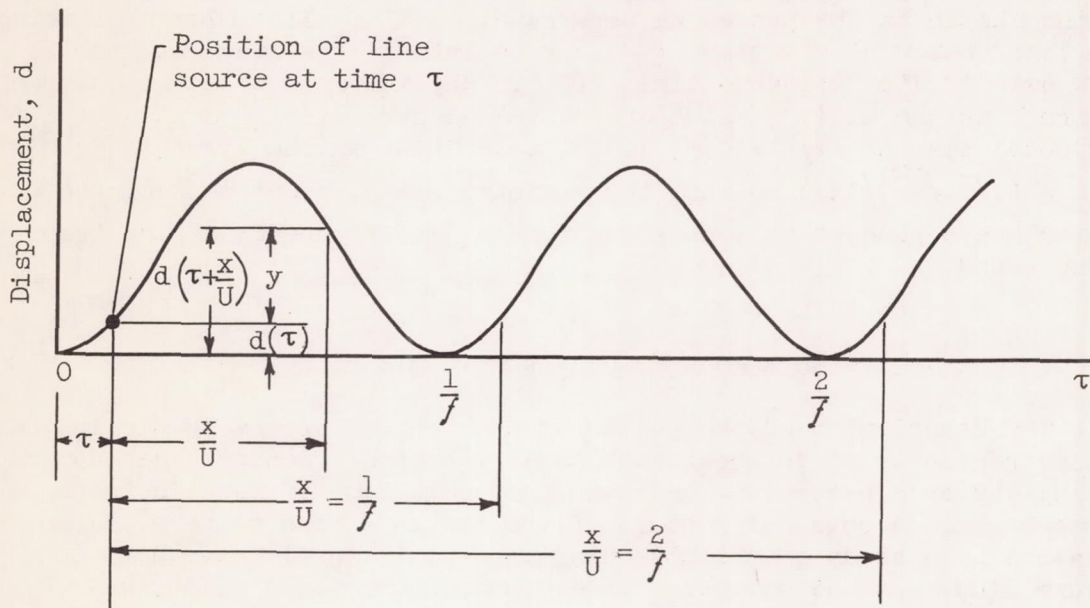
A line element released from the line source at time τ reaches the axial station x after a residence time x/U. The lateral displacement y from the flow-axis plane is given by

$$y = d\left(\tau + \frac{x}{U}\right) - d(\tau) \tag{12}$$

where $d(\tau)$ is d evaluated at time τ and $d(\tau + x/U)$ is d at time $\tau + (x/U)$. By combining equation (11) with equation (12), the time history of the position of the center of the molecular-diffusion wake at any axial station x is

$$y = \frac{\sqrt{2}\sqrt{\overline{v^2}}}{2\pi f} \left\{ \left[1 - \cos\left(2\pi f\tau + 2\pi f\frac{x}{U}\right)\right] - \left[1 - \cos\left(2\pi f\tau\right)\right]\right\} \tag{13}$$

which reduces to

$$y = \frac{\sqrt{2}\sqrt{\overline{v^2}}}{\pi f} \sin\left(\frac{\pi f x}{U}\right) \sin\left(2\pi f \tau + \frac{\pi f x}{U}\right) \tag{14}$$

Figure 1(b) shows the position of the molecular-diffusion-wake center at various times through one cycle of transverse velocity fluctuation. The wake positions are shown only through two nodal points, but theoretically they continue on downstream in the same cyclic fashion. An interesting feature of figure 1(b) is the existence of definite nodal points at $f x/U = 1, 2, \ldots$ The reason for these nodal points is shown by the sketch in the preceding paragraph. A fluid line element leaving the line source at any time τ has zero lateral displacement from the flow axis if its residence time x/U is any multiple of $1/f$. Also of interest is the maximum value of the wake center displacement at the antinodal planes $f x/U = 0.5, 1.5, \ldots$ This maximum value is equal to $y_{max} = \left(\sqrt{2}\sqrt{\overline{v^2}}\right)/(\pi f)$ so that the maximum lateral excursions of the wake center are dependent only on the intensity and frequency of the transverse sound wave.

Instantaneous Temperature in Mixing Region

The description of the instantaneous temperature at points in the mixing region is of interest both as an important factor in aerodynamic mixing and as a preliminary step in the evaluation of the time-mean temperature. A physical picture of the instantaneous temperature may be obtained by a study of the molecular-wake-position diagram shown in figure 1(b). As the molecular wake approaches a fixed point, say P_1, the temperature at the point rises because of the temperature profile of the wake as illustrated in figure 1(a). When the wake center reaches the point, the temperature is at the peak value of the wake profile. Then, as the wake passes on away from the point, the temperature decreases to a minimum which is reached when the wake is at its farthest position from the point. Because the lateral motion of the wake is cyclic, the time history of the instantaneous temperature will also be cyclic with a period equal to that of the lateral velocity fluctuations associated with the standing sound wave.

Typical time histories of instantaneous temperatures are shown in figure 2. The three time histories represent the temperature fluctuations at points P_1, P_2, and P_3 in figure 1(b), and were calculated from a theoretical equation derived later in this section. Consideration of figures 1(a) and (b) shows that the temperature at the nodal lines will be steady in time. Temperatures at other points in the nodal planes

(for instance, point P_4 in figure 1(b)) will have slight periodic changes with time, since the pivoting motion of the wake at the nodal line will act to change the perpendicular distance from the point to the wake center. The remainder of this section is devoted to mathematical statements of the physical picture described in this paragraph.

Exact model for instantaneous temperature. - The exact solution for instantaneous temperature employs a method described in reference 7. The molecular wake downstream from a continuously emitting line source is considered to be a sheet composed of an infinite number of instantaneous line sources. Each of these instantaneous line sources was originally introduced at the continuous line source (the heated wire), and the degree to which it has diffused into its surroundings is a function only of its residence time in the stream, as shown by equation (8). The geometry of the sheet of instantaneous line sources expressed by equation (14) is shown diagrammatically in figure 1(b) and is shown for a partic- ular value of the parameter τ in the following sketch:
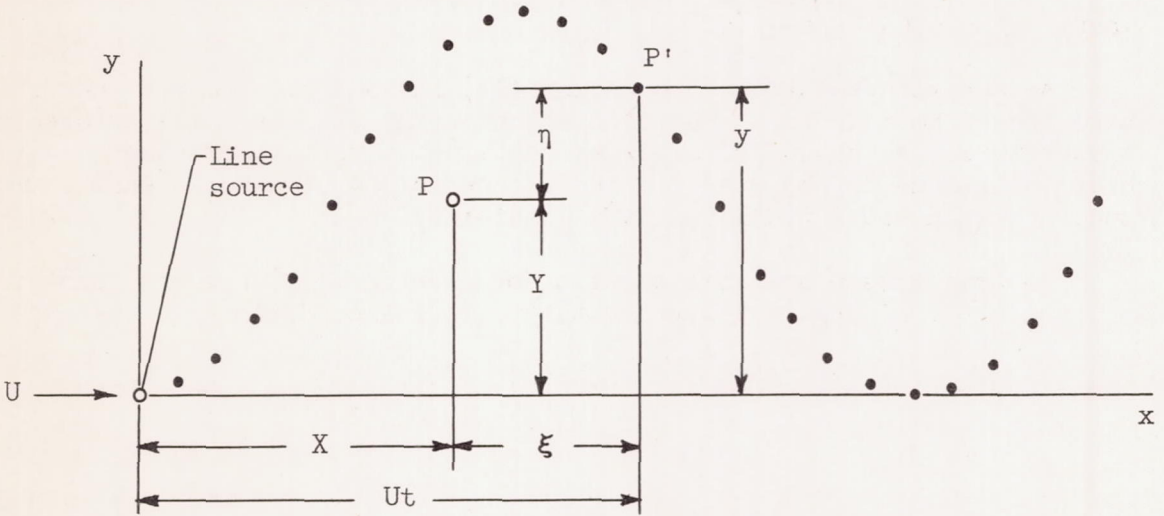
An important feature shown in the preceding sketch is that the density, or proximity, of neighboring instantaneous line sources is decreased when the sheet is distorted. This effect is of consequence in later discussions.

The concentration of heat at the fixed point $P(X,Y)$ at time τ is the summation of contributions of heat from all the instantaneous line sources $P'(Ut,y)$ in the entire sheet. The contribution of heat to $P(X,Y)$ by one instantaneous line source at $P'(Ut,y)$ is

$$dh = \frac{\frac{d(H/l)}{dt}\,dt}{4\pi\omega}\, e^{-\frac{1}{4\omega}\left[(Ut - X)^2 + (y - Y)^2\right]} \tag{15}$$

The total concentration at $P(X,Y)$ is the summation of all contributions:

$$h = \frac{q/l}{4\pi} \int_0^\infty \frac{1}{\omega} e^{-\frac{1}{4\omega}\left[(Ut - X)^2 + (y - Y)^2\right]} dt \tag{16}$$

By employing the functional relations between ω and y and the residence time t (eqs. (5) and (14)) and by changing the independent variable, equation (16) may be written as:

$$h = \frac{q/l}{4\pi\alpha} \int_0^\infty \frac{1}{\pi f t} e^{-\left(\frac{U^2}{4\alpha\pi f}\right)\frac{1}{\pi f t}\left\{\left(\pi f t - \pi f \frac{X}{U}\right)^2 + \frac{2\overline{v^2}}{U^2}\left[\sin(\pi f t)\sin(2\pi f \tau + \pi f t) - \frac{Y}{y_{max}}\right]^2\right\}} d(\pi f t) \tag{17}$$

where $y_{max} = \left(\sqrt{2}\sqrt{\overline{v^2}}\right)/(\pi f)$

An analytic solution to equation (17) has not been found; therefore, resort must be made to a numerical solution for the exact instantaneous temperature. As shown in following sections, a variety of simple algebraic solutions may be used for instantaneous and time-mean temperatures under certain sound-field and flow conditions.

An approximate analytic solution of equation (17) has been made for points in the mixing region under the following conditions:

$$\left.\begin{array}{c} f\dfrac{X}{U} = 4.5, \ 5.5, \ 6.5 \ \ldots \\[2mm] Y = 0 \\[2mm] f\tau = 0.25, \ 0.75, \ 1.25 \ \ldots \\[2mm] \dfrac{U^2}{4\pi^2 f^2 \omega_X}\left(1 + \dfrac{2\overline{v^2}}{U^2}\right) > 50 \end{array}\right\} \tag{18}$$

As shown by the conditions above, the solution is for the maximum instantaneous temperature at the antinodal stations. The solution is derived in appendix B, and its final form is

$$h \approx \frac{q/l}{U\sqrt{4\pi\omega_X}} \frac{1}{\sqrt{1 + \dfrac{2\overline{v^2}}{U^2}}} \qquad \text{(for conditions (18))} \tag{19}$$

where ω_X is evaluated at the time X/U.

Approximate model for small deformation of diffusion wake. -   If the deformation of the molecular-diffusion-wake center is small, an approximate analytic solution can be obtained from the continuous-line-source model defined by equation (9). Two conditions are necessary for the use of this model: (a) stretching of the molecular wake must be small, and (b) the radius of curvature of the deformed molecular-wake center must be large with respect to the molecular-wake thickness. The following sketch illustrates the necessity for these conditions:
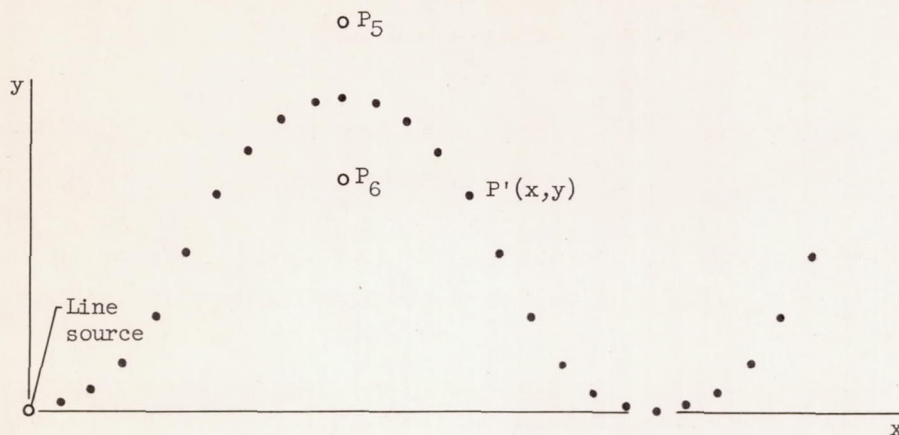
The continuous-line-source model was derived for a perfectly straight molecular-wake center plane, so that the density, or spacing, of instantaneous line sources along the wake was constant, or uniform. As shown by the preceding sketch, stretching of the wake causes a departure from constant source density. The criterion for condition (a) is that the ratio $\dfrac{S - (U/f)}{(U/f)}$ must be nearly zero, where S is the stretched length between nodal points and (U/f) is the direct distance between nodal points. This ratio is derived in appendix B, and its final form is

$$\frac{S - \left(\dfrac{U}{f}\right)}{(U/f)} = \frac{2}{\pi}\left(1 + \frac{2\overline{v^2}}{U^2}\right)^{1/2} \mathscr{E} - 1 \tag{20}$$

where $\mathscr{E}$ is the elliptic integral and is defined as

$$\mathscr{E} = \int_0^{\frac{\pi}{2}} \left[1 - \left(\frac{1}{\dfrac{U^2}{2\overline{v^2}} + 1}\right) \sin^2 \varphi\right]^{1/2} d\varphi \tag{21}$$

Equations (20) and (21) show that the stretching is a function only of the ratio $\sqrt{\overline{v^2}}/U$. This functional relation is shown in figure 3(a).

Consideration of the previous sketch shows that the points P_5 and P_6 receive contributions of different magnitudes from P' and that the total contributions received by P_6 are greater than those received by P_5. Therefore, to approximate the continuous-line-source model, condition (b) is necessary. The minimum radius of curvature $r_{C,min}$ for any time in the cycle is derived in appendix B and has the following value:

$$r_{C,min} = \frac{U^2}{2\sqrt{2}\ \pi f \sqrt{\overline{v^2}}} \tag{22}$$

This value occurs when $2\pi f \tau + 2\pi f \frac{X}{U} = \pi, 2\pi, 3\pi, \ldots$ Condition (b) is satisfied when $r_{C,min} \gg \sqrt{\omega}$. The minimum radius of curvature is plotted in figure 3(b) for a range of values of the parameters $\sqrt{\overline{v^2}}/U$ and U/f. The effect of distance downstream on the ratio $r_{C,min}/\sqrt{\omega}$ is shown in figure 3(c) for a particular value of the coefficient of thermal diffusivity α.

If conditions (a) and (b) are satisfied, then an expression for instantaneous temperature can be derived from equation (9). Figure 4 is a diagram of the molecular-wake position with respect to a fixed point, where the distance from the wake center to the fixed point is η. Since the radius of curvature is large, the distance η is approximated by

$$\eta \approx (y - Y)\sin\left(\text{arc cot } \frac{dy}{dx}\right) \tag{23}$$

which may be written

$$\eta \approx \frac{y - Y}{\sqrt{\left(\frac{dy}{dx}\right)^2 + 1}} \tag{24}$$

Substituting for the lateral distance η in equation (9) and using equation (14) for y result in

$$h \approx \frac{q/l}{U\sqrt{4\pi\omega_x}}\ e^{-\frac{1}{4\omega_x}\left\{\frac{\left[\frac{\sqrt{2}\sqrt{\overline{v^2}}}{\pi f}\sin\left(\frac{\pi f X}{U}\right)\sin\left(2\pi f \tau + \frac{\pi f X}{U}\right) - Y\right]^2}{1 + \frac{2\overline{v^2}}{U^2}\sin^2\left(2\pi f \tau + 2\pi f \frac{X}{U}\right)}\right\}} \tag{25}$$

which may be reduced to

$$h \approx \frac{q/l}{U\sqrt{4\pi\omega_x}}\, e^{-\dfrac{\overline{v^2}}{2\pi^2 f^2 \omega_x}\dfrac{\left[\sin\left(\dfrac{\pi f X}{U}\right)\sin\left(2\pi f \tau + \dfrac{\pi f X}{U}\right) - \dfrac{Y}{y_{max}}\right]^2}{\left[1 + \dfrac{2\overline{v^2}}{U^2}\sin^2\left(2\pi f \tau + 2\pi f \dfrac{X}{U}\right)\right]}} \tag{26}$$

If the ratio $\sqrt{\overline{v^2}}/U$ is very small, then dy/dx is negligible, and the solution becomes

$$h \approx \frac{q/l}{U\sqrt{4\pi\omega_x}}\, e^{-\dfrac{\overline{v^2}}{2\pi^2 f^2 \omega_x}\left[\sin\left(\dfrac{\pi f X}{U}\right)\sin\left(2\pi f \tau + \dfrac{\pi f X}{U}\right) - \dfrac{Y}{y_{max}}\right]^2} \tag{27}$$

For cases where ρc_p is nearly constant over the temperature range of interest, equation (2) may be replaced by $h = \rho c_p\, \Delta T$, and equations (26) and (27) may be written, respectively,

$$\Delta T \approx \Delta T_0\, e^{-\dfrac{\overline{v^2}}{2\pi^2 f^2 \omega_x}\dfrac{\left[\sin\left(\dfrac{\pi f X}{U}\right)\sin\left(2\pi f \tau + \dfrac{\pi f X}{U}\right) - \dfrac{Y}{y_{max}}\right]^2}{\left[1 + \dfrac{2\overline{v^2}}{U^2}\sin^2\left(2\pi f \tau + 2\pi f \dfrac{X}{U}\right)\right]}} \tag{28}$$

$$\Delta T \approx \Delta T_0\, e^{-\dfrac{\overline{v^2}}{2\pi^2 f^2 \omega_x}\left[\sin\left(\dfrac{\pi f X}{U}\right)\sin\left(2\pi f \tau + \dfrac{\pi f X}{U}\right) - \dfrac{Y}{y_{max}}\right]^2} \tag{29}$$

where $\Delta T_0 = (q/l)/(U\rho c_p\sqrt{4\pi\omega_x})$ and $y_{max} = \left(\sqrt{2}\,\sqrt{\overline{v^2}}\right)/(\pi f)$. The instantaneous-temperature variations shown in figure 2 were calculated from equation (29).

Another version of the approximate model is described in appendix B. In this version, the distance η shown in figure 4 is determined analytically.

Time-Mean Temperature in Mixing Region

The time-mean temperature at any point in the mixing region may be obtained by averaging the instantaneous temperature over one period of its cyclic fluctuation:

$$\overline{\Delta T} = f \int_0^{1/f} \Delta T \, d\tau = \int_0^1 \Delta T \, d(f\tau) \tag{30}$$

where the bar denotes a long-time average. The analysis employs equations from the preceding sections, which are written in terms of the volume specific enthalpy and can be converted to the temperature difference $\Delta T = T - T_{am}$ by means of equation (2). Typical time-mean temperature profiles are shown in figure 5 for the case of small deformation of the molecular-diffusion wake. An important feature of the time-mean temperature profiles is that the mean temperature values are higher near the outer edges of the profiles. This is due to the lower transverse velocity of the wake center at its extreme excursions. This point is illustrated in figure 2 by inspection of the relative magnitudes of areas under the temperature variations at the points P_1, P_2, and P_3. Another feature of figure 5 is the absence of aerodynamic mixing at the nodal points $fx/U = 1, 2, \ldots$

Calculation of mean temperature for exact model. - Since an analytic solution was not found for the instantaneous temperature fluctuations of the exact model (eq. (17)), a graphical integration method must be employed for evaluation of the mean temperature. Equation (17) may be solved graphically for any fixed point $P(X,Y)$ and for a series of times τ. Then through equation (2), the instantaneous temperature difference at the fixed point $P(X,Y)$ may be plotted as a function of the time τ. The mean temperature difference $\overline{\Delta T}$ can then be obtained graphically.

Mean temperature for small deformation of diffusion wake. - Calculation of time-mean temperature for the case of small wake deformation is somewhat simpler than for the exact model, since approximate analytic solutions are derived for this case in preceding sections. Instantaneous temperature variations, such as those of figure 2, may be plotted from equations (28) or (29), and the time-mean temperature may be evaluated graphically from such plots.

Approximate analytic solutions for the mean temperature have been obtained from equation (29). The derivations of these solutions and the assumptions necessary for their validity are detailed in appendix B. The approximate solutions are for the two zones in the mixing region shown in the following diagram:
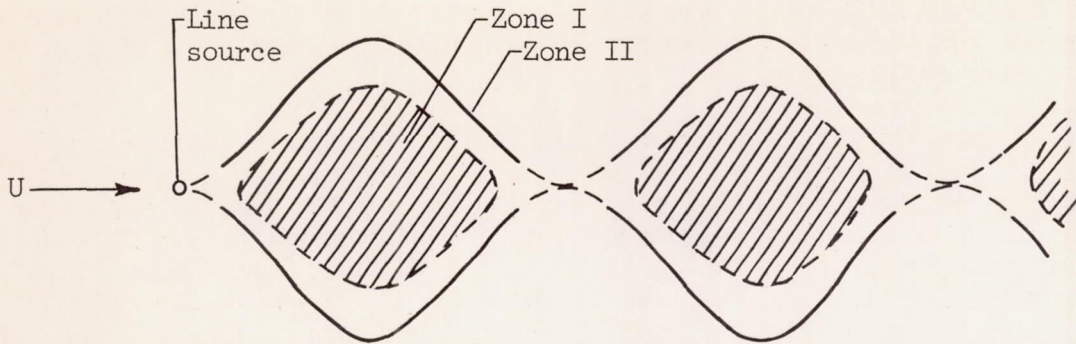
where zone I lies within the extreme wake position and zone II lies along the extreme wake position. The approximate solutions for zones I and II are, respectively,

$$\overline{\Delta T} \approx \frac{q/l}{2\sqrt{2}\rho c_p \sqrt{1-R^2}}\left[\frac{f}{\sqrt{\overline{v^2}}\ U\left|\sin\left(\pi f\frac{X}{U}\right)\right|}\right]\left(\left[1+\frac{1}{4F(1-R^2)}\right]\left\{\text{erf}\left[\sqrt{F}\ (1+R)\right]\ +\right.\right.$$

$$\left.\text{erf}\left[\sqrt{F}\ (1-R)\right]\right\} - \frac{1}{\sqrt{\pi F}(1-R)}\left.\left[\frac{1-R}{1+R}\ e^{-F(1+R)^2}+e^{-F(1-R)^2}\right]\right)$$

$$\text{(Zone I)} \qquad (31)$$

$$\overline{\Delta T} \approx \frac{\sqrt{2}}{F^{0.25}}\frac{\Delta T_0}{\pi}\ \Gamma(1.25) \qquad \text{(Zone II)} \qquad\qquad (32)$$

where $F = \dfrac{\overline{v^2}\sin^2\left(\pi f\frac{X}{U}\right)}{2\pi^2 f^2 \omega_x}$ and $R = \dfrac{Y\ \pi f}{\sqrt{2}\ \sqrt{\overline{v^2}}\sin\left(\pi f\frac{X}{U}\right)} = \dfrac{Y}{y_{max}\sin\left(\pi f\frac{X}{U}\right)}$

Close inspection of equation (31) shows that the time-mean temperature $\overline{\Delta T}$ in zone I is affected by the sound field and stream parameters in the following ways when $\sqrt{F}(1-R) > 2$: (a) $\overline{\Delta T}$ increases as the sound-wave frequency rises; (b) $\overline{\Delta T}$ decreases as the sound intensity rises; and (c) $\overline{\Delta T}$ decreases as the stream velocity rises. Equations (31) and (32)

may be used to construct time-mean temperature profiles such as shown in figure 5 by fairing between zones I and II. As pointed out in the RESULTS AND DISCUSSION, the peak value of $\overline{\Delta T}$ occurs between zones I and II, which should be kept in mind when fairing the profile.

Analytic Procedure for Nonsinusoidal Velocity Fluctuations

In many sound fields, particularly those of extremely high intensity, the velocity fluctuations may depart from sinusoidal form. The analytic procedure for this situation is identical to that followed previously in the text. If the mathematical expression for the variation of velocity fluctuation with time is known, then analytic expressions for the instantaneous and time-mean temperatures might be found. If the velocity fluctuation does not follow a known mathematical relation with time, then graphical, or numerical, solutions for the instantaneous and time-mean temperatures may be made by following the steps in the analytic procedure discussed previously. The graphical method is outlined in the SUMMARY OF RESULTS AND THEIR PRACTICAL APPLICATION.

APPARATUS AND EXPERIMENTAL PROCEDURE

Flow and Sound-Field Measurements

The apparatus used to produce a standing sound wave transverse to a low-turbulence airstream is shown in figure 6. The calming chamber minimized the effect of room drafts on the stream velocity and static temperature. The stream velocity was controlled by the adjustable-area exhaust valve. The standing sound wave was generated by acoustical driver units located at opposite ends of the resonant chamber (as shown in fig. 6). The opposing groups of driver units were connected electrically 180° out of phase and were powered by a 1400-watt oscillator amplifier. The line source of heat was a 0.003-inch-diameter Advance wire continuously heated by direct current. Calculations of radiation and end conduction showed that these losses were negligible.

The stream velocity, static temperature, static pressure, transverse velocity fluctuations, and sound-wave frequency were measured as described in appendix C. These parameters were held constant during the experiment at the following values:

Stream velocity, U, ft/sec 17.6
Ambient static temperature, T_{am}, °F . . . . 75 to 82
Static pressure, in. Hg abs . . . . 29.0 to 29.7
Root-mean-square transverse velocity fluctuation, $\sqrt{\overline{v^2}}$, ft/sec . . 3.33
Sound pressure level, db 147
Sound-wave frequency, f, cps 104
Heat addition from line source, q/l, Btu/(ft)(sec) 0.0308

Instantaneous and Time-Mean Temperature Measurements

Two different methods, resistance thermometry and hot-wire anemometry, were used to measure the instantaneous temperature downstream from the line source of heat. These instantaneous temperature measurements were made at several transverse positions in the mixing wake at the axial station $fX/U = 1.47$.

The sensitive element of the resistance thermometer was a standard hot-wire-anemometer probe. The resistance thermometer was essentially sensitive only to temperature fluctuations in the airstream. Equations describing this instrument's sensitivity and the compensating circuit are given in appendix D. The anemometer probe also was operated as a constant-temperature hot-wire anemometer. The hot-wire anemometer was sensitive to both temperature and velocity fluctuations in the stream. Details of the hot-wire technique and the sensitivity equations are in appendix E.

The mean temperatures at points in the mixing region were measured with a thermopile probe as described in appendix F. The mean-temperature measurements were made at several transverse positions at the following axial stations: $fX/U = 0.24$, 0.50, 0.75, 1.00, 1.24, 1.47, 1.72, and 1.96.

RESULTS AND DISCUSSION

For the experimental conditions investigated, the stretching of the molecular-diffusion wake was small, and the minimum radius of curvature was large compared with the wake thickness. Because of apparatus limitations, experimental verification of the theoretical analysis was possible only for the case of small deformation of the diffusion wake. However, since large deformations of the diffusion wake are also of practical interest, this case also is discussed herein on the basis of the theoretical analysis alone.

Mixing Data and Comparison with Theory for Small

Deformation of Diffusion Wake

Flow and sound-field measurements. - Flow and sound-field measurements were made throughout the region encompassing two nodal stations downstream from the line source of heat and transverse distances greater than the maximum excursions of the diffusion wake. Measurements with a total-static pitot tube and a hot-wire anemometer showed that the axial stream velocity was constant throughout the region of interest. The hot-wire measurements also showed that the stream turbulence was negligible and that no vortex street existed downstream from the line source.

Measurements with the X-wire anemometer showed that the transverse velocity fluctuation v in the sound field was nearly sinusoidal and that $\sqrt{\overline{v^2}}$ was substantially constant in the region of interest. A typical oscillogram of the transverse velocity fluctuation is shown in figure 7(a), and an axial profile of $\sqrt{\overline{v^2}}$ is shown in figure 7(b). The decrease in $\sqrt{\overline{v^2}}$ at the inlet and exit of the resonant chamber was due to sound leakage through the openings and sound absorption by the chamber walls.
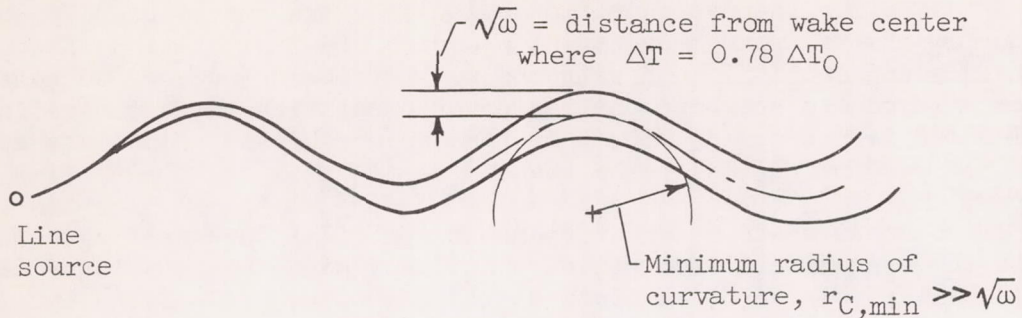
For the conditions used in the experimental investigation, the stretching, radius of curvature, and slope effects had the following values:

$$\frac{S - (U/f)}{(U/f)} = 0.019$$

$$r_{C,min} / \sqrt{\omega_{x,max}} = 54.3$$

$$\frac{dy}{dx}_{max} = 0.19$$

These values were obtained from figures 3(a) and (b) for the measured values of $\sqrt{\overline{v^2}}$, U, and $\omega_{x,max}$ ($\omega_{x,max}$ is the maximum value of ω, calculated at the maximum value of X). The values show that the theoretically predicted wake deformation was negligibly small, as illustrated by the following sketch:

$\sqrt{\omega}$ = distance from wake center
where $\Delta T = 0.78 \, \Delta T_0$

Line
source

Minimum radius of
curvature, $r_{C,min} \gg \sqrt{\omega}$

Instantaneous temperatures were calculated from the exact model (eq. (17)) and the approximate model (eq. (29)) for the experimental conditions. These calculations showed very close agreement; therefore, the stretching and curvature parameters listed above may be considered representative for the case of small wake deformation.

Instantaneous-temperature measurements and comparison with theory. - Instantaneous-temperature measurements were made at the second antinodal station ($fX/U = 1.47$) with both the resistance-thermometer and hot-wire-anemometer techniques. Typical oscillograms made by these two methods are shown in figures 8(a) and (b), respectively. The measurements were made at three transverse positions, $Y/y_{max} = 0$, 0.49, and 0.98, and show good agreement in shape. The hot-wire-anemometer results are discussed further in appendix E.

Instantaneous-temperature variations were calculated from the resistance-thermometer oscillograms of figure 8(b). These experimental instantaneous-temperature variations are compared in figure 9 with the theoretical analysis for small deformations of the diffusion wake as expressed by equation (29). Since the transverse velocity fluctuations were not precisely sinusoidal, graphical solutions were also made and plotted in figure 9. These solutions were based on oscillograms such as figure 7(a) and followed the methods outlined by the theoretical analysis. The agreement between the experimental data and the theoretical and graphical solutions is quite good at the transverse positions $Y = 0$ and $Y = 0.17$ inch. The discrepancy in figure 9(b) may be due to error in the probe position. The peaks in the measured temperature fluctuation are closer to $f\tau = 0$ than are the theoretical curves, and the measured instantaneous temperature is higher than the theoretical value at $f\tau = 0$. Inspection of figure 2 shows that these two observations are consistent with an error in probe position. The asymmetry of the theoretical curves about $f\tau = 0$ in figure 9 is due to the fact that fX/U was not an exact antinode. Calculation shows that the theoretical curve is symmetric about $f\tau = 0.016$.

Time-mean temperature measurements and comparison with theory. - Time-mean temperatures measured with the thermopile probe are compared with theoretical analyses in figure 10. The transverse profiles of time-mean temperature were measured at a series of axial stations through the second nodal station, both with and without the transverse sound field. The measured temperatures show good agreement with the equation for molecular diffusion (eq. (9)), in the absence of the transverse sound field.

The measured time-mean temperature profiles show good agreement with the approximate theoretical solutions, given by equations (31) and (32), except at the axial stations $fX/U = 0.75$, 1.00, 1.72, and 1.96, as shown by figures 10(c), (d), (g), and (h), respectively. At the stations $fX/U = 1.00$ and 1.96, the measured profiles indicate some degree of mixing, contrary to the theoretical prediction of no mixing at the nodal stations. The measured profiles at stations $fX/U = 0.75$ and 1.72 indicate less mixing than theoretically predicted. These discrepancies may be due to probe positioning error or to errors in the measurement of stream velocity U and sound-wave frequency f through which the theoretical nodal stations $fX/U = 1, 2, \ldots$ are determined.

The interpolation between the theoretical solutions given by equations (31) and (32) is shown by the dotted lines in figure 10. The maximum values of $\overline{\Delta T}$ fall at values of Y/y_{max} less than 1.0. This is because at a point Y/y_{max} less than 1.0 the wake passes twice in a cycle; and, if the point is near $Y/y_{max} = 1.0$, the wake passes at a velocity less than that at $Y/y_{max} = 0$. Calculations of time-mean temperature from the exact model (eqs. (17) and (30)) showed that the peak values of $\overline{\Delta T}$ fell close to $Y/y_{max} = 1.0$, as shown in figure 10.

By closer inspection of figure 10, it can be seen that the agreement between theory and experiment is particularly good near the line source of heat and at the antinodal stations. It is possible that a random angular fluctuation in the stream direction might explain the disagreement between theory and experiment at far downstream stations where the lateral displacements of the wake are small. This possibility is strengthened by the observation of low-frequency random fluctuations in the thermopile-probe emf readings throughout the course of the experiment.

Graphical solutions, based on the velocity fluctuation oscillograms (fig. 7(a)), were made for the axial stations $fX/U = 0.75$ and 1.47 as shown in figures 10(c) and (f), respectively. These graphical solutions are in fairly good agreement with the analytic solutions based on a sinusoidal velocity wave form, so the nonsinusoidal wave form was not the reason for disagreement between theory and experiment.

The discrepancies discussed appear to be caused by imperfect experimental conditions and techniques. For this reason, the experimental data are considered to be satisfactory substantiation of the theoretical analysis for small deformation of the diffusion wake.

Theoretical Effect of Large Diffusion-Wake Deformations on Mixing

In order to illustrate the effect of wake deformation on the instantaneous and time-mean aerodynamic mixing, a comparison was made between the exact model and solutions applying in the case of negligible wake deformation. The exact model (eq. (17)) accounts fully for stretching and curvature of the wake. The solutions for negligible wake deformation (eqs. (29), (28), and (B40)) are predicated on the assumptions of negligible wake stretching and negligible diffusion in the stream (axial) direction. In addition, equation (29) assumes that the wake center is nearly parallel to the stream direction (i.e., small slope), and equation (28) assumes that the wake center has negligible curvature. Equation (B40) accounts for the geometric curvature of the wake and is derived in appendix B.

In order to determine the effect of appreciable wake deformation on the mixing parameters ΔT and $\overline{\Delta T}$, solutions from the exact and approximate models were calculated for the following conditions:

$$\sqrt{\overline{v^2}} = 16.7 \text{ fps } (161 \text{ db})$$

$$f = 520 \text{ cps}$$

$$U = 17.6 \text{ fps}$$

$$q/l = 0.0308 \text{ Btu}/(\text{ft})(\text{sec})$$

$$f X/U = 7.5$$

These conditions were chosen so that the seventh antinode $(f X/U = 7.5)$ fell at the same axial station as the second antinode in the experiment. This kept the width of the molecular wake the same as in the experiment. The conditions above are also such that y_{max} is the same as in the experiment so that a graph of ΔT against $f\tau$ would show local mixing in space. The stretching and curvature parameters for the conditions above are

$$\frac{S - (U/f)}{(U/f)} = 0.36$$

$$r_{C,min}/\sqrt{\omega_{max}} = 2.17$$

   Effect on instantaneous temperature. - Instantaneous-temperature
differences ΔT were calculated from the exact model (eq. (17)), for
the conditions above, at a series of transverse positions. These instan-
taneous temperatures are shown by the solid lines in figures 11(a) to
(d). For comparison with the exact model, instantaneous-temperature
differences were calculated for the same conditions from the simplest
solution of the small-deformation model as given by equation (29). The
small-deformation-model solution is shown by the short-dash lines in
figures 11(a) to (d). This comparison of exact and approximate models
clearly shows that a substantial degree of instantaneous, or local,
mixing occurs when the wake deformations are large. For all the trans-
verse positions shown, the peak temperature of the instantaneous time
profile is substantially lower when the wake is deformed. This decrease
in peak temperature is due to the stretching of the wake and concurrent
lower density of instantaneous sources, as discussed in the THEORETICAL
ANALYSIS. The decrease is largest for the transverse position $Y = 0$,
since the source density is lowest for the shape assumed by the wake as
it passes through $Y = 0$ at an antinodal station. This point can be
verified from inspection of the sketches in the THEORETICAL ANALYSIS
section and of figure 4.

   In order to illustrate the effect of curvature, equation (28) is
plotted in figure 11 as a broken line. Equation (28) accounts for the
slope of the wake center, thereby being a more accurate representation
of the small-deformation model. In addition, a precise representation
of the small-deformation model is shown in figure 11 by the long-dash
lines. This solution (eq. (B40)) accounts fully for the geometric curva-
ture of the wake center, as shown in figure 4, and is derived in appendix
B. The effect of curvature on the exact model is illustrated in figure
11(c). By inspection of figure 1(b), it is seen that a fixed point at
$Y/y_{max} = 0$ in the antinodal plane receives significant contributions
from a longer arc length of the wake when the wake is at $f\tau = 0$ than
when the wake is at $f\tau = 0.15$. Because of this curvature effect on
contributions to $Y/y_{max} = 0.8$, the exact model shows a correct tempera-
ture at $f\tau = 0$ which is higher than any of the solutions to the small-
deformation model. This behavior of the exact model in comparison to
that of the small-deformation model is quite reasonable in view of the
fact that the small-deformation model implicitly assumes a flat, uncurved,
center shape.

   The peak-instantaneous-temperature difference calculated from
equation (19) is also shown in figure 11(a). The comparison of equation
(19) with equation (17) is quite good, indicating that equation (19) may
be used for approximate calculation of the peak instantaneous temperature
for the case of large wake deformation. Algebraic comparison of equa-
tions (19) and (27) shows that the peak temperature at the antinodal
stations and $Y = 0$ is diminished approximately by the factor

$1/\sqrt{1 + 2\overline{v^2}/U^2}$ when wake deformation becomes appreciable.

In summary, large wake deformations substantially lower the peak values of the instantaneous temperature and appreciably change the shape of the temperature-time profile.

Effect on time-mean temperature. - The effect of wake stretching and curvature on the time-mean temperature is shown in figure 12, where theoretical temperature differences $\overline{\Delta T}$ are plotted against the transverse position Y/y_{max}. The values of mean temperature difference were calculated from equation (30) for each of the four solutions shown in figures 11(a) to (d).

As discussed in the preceding section, equation (B40) is the precise representation of temperature fluctuations for the case of negligible wake deformation. The mean temperatures calculated from the exact model (eqs. (17) and (30)) are considerably lower than those calculated from the negligible deformation model (eqs. (B40) and (30)). This comparison clearly shows the effect of stretching and curvature on the time-mean mixing.

The instantaneous-temperature variations calculated from the negligible deformation model (eq. (29)) are very different from those calculated from the exact model (eq. (17)), as shown in figure 11. For this reason, the close agreement between the mean temperature differences calculated from these two models and shown in figure 12 is fortuitous.

In summary, large wake deformations substantially lower the time-mean temperatures throughout the transverse profiles in the mixing region.

SUMMARY OF RESULTS AND THEIR PRACTICAL APPLICATION

In order to facilitate the engineering application of the information presented in this report, the results are summarized in this section. The information is divided into four practical problem cases: for sound fields with a sinusoidal wave form (1) for small wake deformation and (2) for large wake deformation, and for sound fields with a nonsinusoidal wave form (3) for small wake deformation and (4) for large wake deformation. The criteria for small wake deformation are low values of the stretching parameter $\frac{S - (U/f)}{(U/f)}$, which can be evaluated from figure 3(a), and high values of the curvature parameter $r_{C,min}/\sqrt{\omega_{max}}$, where the radius of curvature $r_{C,min}$ can be evaluated from figure 3(b) and the spreading coefficient ω can be evaluated from equation (5). If $r_{C,min}/\sqrt{\omega_{max}}$ is greater than 50, then the effect of curvature is negligible.

Another criterion for small wake deformation is the comparison of peak instantaneous temperatures at the antinodal stations and $Y = 0$ calculated from equations (19) and (27). (Note conditions imposed on eq. (19) in the THEORETICAL ANALYSIS section.) This comparison shows that if $(2\overline{v^2}/U^2) \approx 0$, then the peak temperatures calculated from these two equations are nearly equal and the wake deformation is small.

In the sections following, equations and procedures are listed for each of the four cases discussed previously.

Sound Fields with Sinusoidal Wave Form

Small wake deformation. - The conditions necessary for small wake deformation are

$$\frac{S - (U/f)}{(U/f)} \approx 0$$

$$r_{C,min} >> \sqrt{\omega_{max}}$$

$$\frac{\sqrt{\overline{v^2}}}{U} \approx 0$$

Recommended equations:

$$\Delta T(X,Y,\tau) = \Delta T_0 \, e^{-\frac{\overline{v^2}}{2\pi^2 f^2 \omega_X}\left[\sin\left(\frac{\pi f X}{U}\right)\sin\left(2\pi f\tau + \frac{\pi f X}{U}\right) - \frac{\pi f Y}{\sqrt{2}\sqrt{\overline{v^2}}}\right]^2}$$

(29)

$$\overline{\Delta T}(X,Y) \approx \frac{\Delta T_0}{2\sqrt{\pi F}\sqrt{1-R^2}}\left(\left[1 + \frac{1}{4F(1-R^2)}\right]\left\{\mathrm{erf}\left[\sqrt{F}(1+R)\right] + \mathrm{erf}\left[\sqrt{F}(1-R)\right]\right\} - \right.$$

$$\left. \frac{1}{\sqrt{\pi F}(1-R^2)}\left[\frac{1-R}{2}\,e^{-F(1+R)^2} + \frac{1+R}{2}\,e^{-F(1-R)^2}\right]\right) \qquad \text{(zone I)}$$

(B28)

$$\overline{\Delta T}(X,Y) \approx \frac{\sqrt{2}}{F^{0.25}}\frac{\Delta T_0}{\pi}\,\Gamma(1.25) \qquad \text{(zone II)} \qquad (32)$$

Large wake deformation:

$$h(X,Y,\tau) = \frac{q/l}{4\pi\alpha} \int_0^\infty \frac{1}{\pi f t} \, e^{-\left(\frac{U^2}{4\alpha\pi f}\right)\frac{1}{\pi f t}\left\{\left(\pi f t - \pi f \frac{X}{U}\right)^2 + \frac{2\overline{v^2}}{U^2}\left[\sin(\pi f t)\sin(2\pi f\tau + \pi f t) - \frac{\pi f Y}{\sqrt{2}\sqrt{\overline{v^2}}}\right]^2\right\}} \, d(\pi f t)$$

$$(17)$$

From equations (17) and (2), plot $\Delta T(X,Y,\tau)$ against τ. Then:

$$\overline{\Delta T}(X,Y) = f \int_0^{1/f} \Delta T \, d\tau \qquad (30)$$

Sound Fields with Nonsinusoidal Wave Form

Small wake deformation. - Conditions necessary:

$$\frac{S - (U/f)}{(U/f)} \approx 0$$

$$r_{C,min} >> \sqrt{\omega_{max}}$$

$$\frac{\sqrt{\overline{v^2}}}{U} \approx 0$$

Recommended procedure:
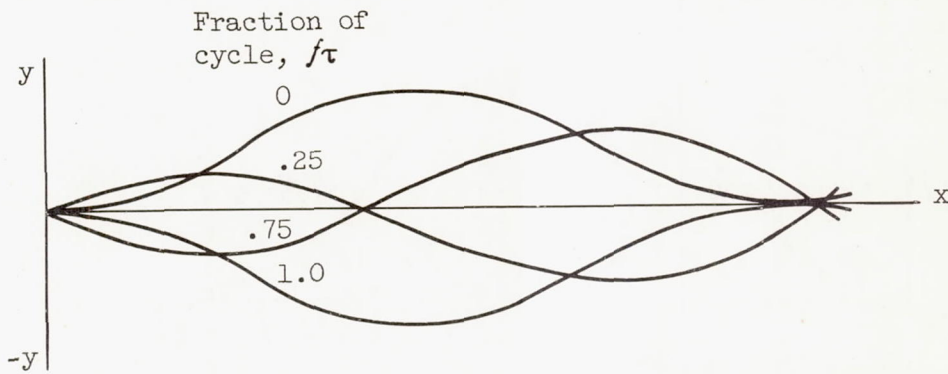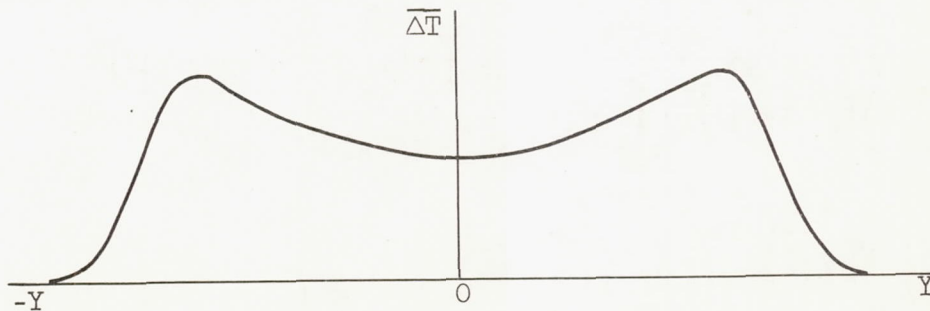
From:
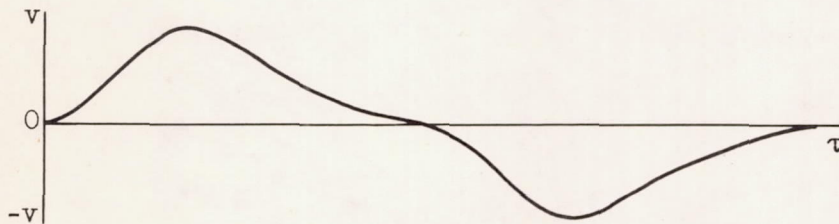
perform graphical integration to obtain:
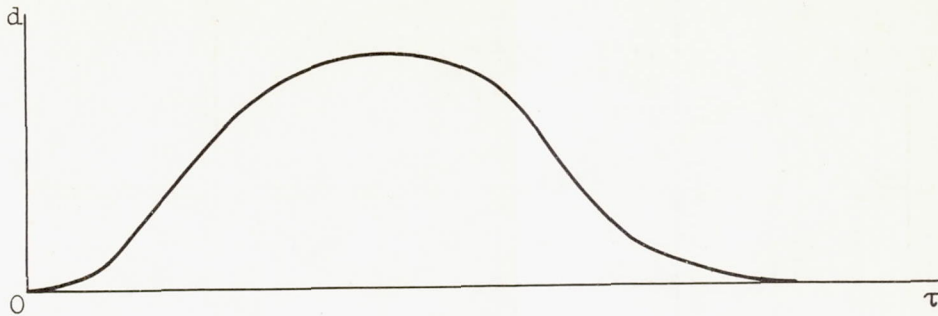
Using equation (12), plot $y(x,\tau)$:

For a particular X and Y, by using equations (9) and (2) and method shown in figure 4 and described by equation (B40), find:
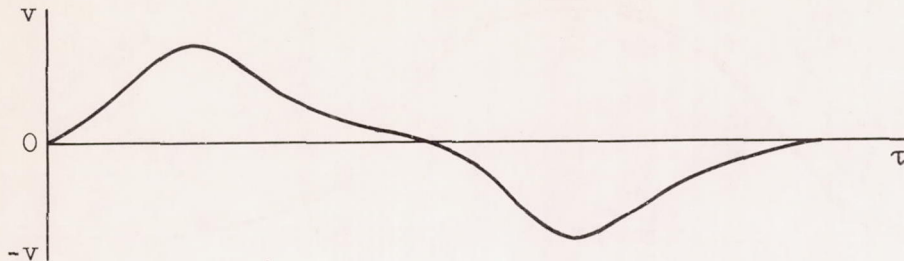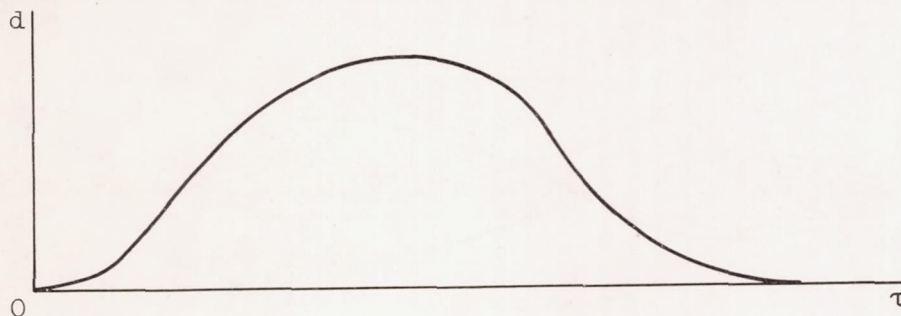

By graphical integration, obtain, for a particular X,
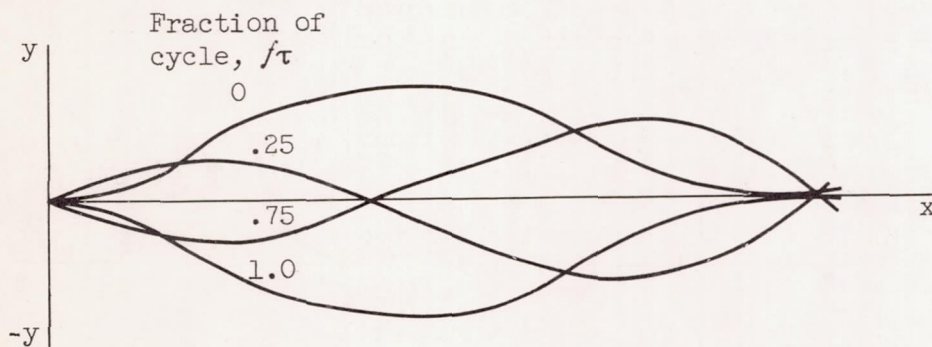
Large wake deformation. - Recommended procedure:

From:

perform graphical integration to obtain:
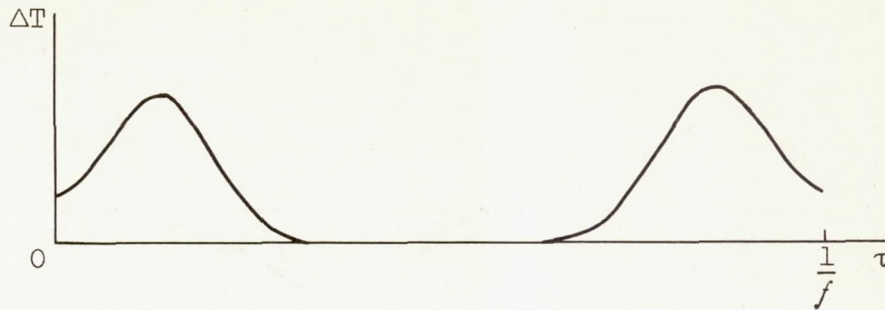

Using equation (12), plot $y(x,\tau)$

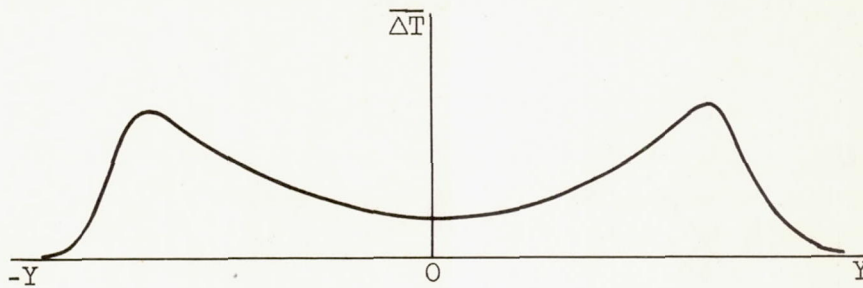Use equation (16) with y for values of Ut from preceding sketches:

$$h(X,Y,\tau) = \frac{q/l}{4\pi}\int_0^\infty \frac{1}{\omega}\, e^{-\frac{1}{4\omega}\left[(Ut - X)^2 + (y - Y)^2\right]}\, dt \qquad (16)$$

For a particular X and Y, from equations (16) and (2), plot:

For a particular X, by graphical integration, find:

CONCLUSIONS

From an investigation of the aerodynamic mixing by a standing sound wave downstream from a continuous line source of heat, the following conclusions are drawn:

1. The velocity fluctuations in a periodic sound field contribute to aerodynamic mixing by periodically displacing the diffusion wake in a manner similar to the displacements of a flag waving in a harmonic mode. Important characterizing parameters of the wake displacement in a sinusoidal-wave-form sound field are:

    a. Nodal points of the wake displacement exist at the stations $fx/U = 1, 2, \ldots$

    b. The maximum wake displacement occurs at the antinodal stations and is equal to ($\sqrt{2}$ × rms transverse velocity fluctuation) divided by (π × sound-wave frequency).

2. When the stretching of the diffusion wake is small and its radius of curvature is much greater than its thickness, then the wake deformation is small, and the sound field has the following mixing effects:

a. In the time-mean sense, concentrations are greatly reduced, except at the nodal stations. For example, near the line source the time-mean temperature difference is reduced by more than an order of magnitude in the presence of a 147-decibel, 104-cycle-per-second sound field.

b. In the instantaneous, or local, sense the sound field does not contribute to mixing.

3. When the sound field causes appreciable deformation of the diffusion wake by stretching and bending, then the sound field contributes to mixing in both the time-mean and instantaneous senses. For example, the peak instantaneous temperature difference in a 161-decibel, 520-cycle-per-second sound field was 61 percent of the peak instantaneous-temperature difference in a 147-decibel, 104-cycle-per-second sound field; and the mean temperature was as low as 66 percent of that in the 147-decibel field.

Lewis Flight Propulsion Laboratory
    National Advisory Committee for Aeronautics
        Cleveland, Ohio, May 9, 1956

APPENDIX A

SYMBOLS

A   term in King's eq.

a   constant in King's eq.

B   term in King's eq.

b   constant in King's eq.

C   capacitance

$\mathscr{C}$ concentration of mass

c_p specific heat at constant pressure

D_M coefficient of molecular diffusion of mass

$\mathscr{D}$ hot-wire diameter

d   transverse displacement of fluid line elements

db   sound pressure level in decibels = $20 \log_{10}$ $\left[p/(0.0002 \text{ dynes/sq cm}) \right]$

E   direct-current voltage

$\mathscr{E}$ complete elliptic integral of second kind

e   alternating-current voltage

erf(x)   error function = $(2/\sqrt{\pi}) \int_0^X e^{-\lambda^2} \, d\lambda$

F   factor equal to $\left[\overline{v^2} \sin^2\left(\frac{\pi f X}{U}\right) \right] \bigg/ (2\pi^2 f^2 \omega)$

f   constant

f frequency

G   electronic gain

g   constant

H/l strength of instantaneous heat line source per unit length

h   volume specific enthalpy (enthalpy per unit volume)

I   direct current

k   thermal conductivity

l length

M   time constant

m   constant in expression for film temperature

P   fixed point in mixing region

P'   position of instantaneous line sources in molecular-diffusion wake

p   sound pressure fluctuation

q/l rate of heat release from line source per unit length

R   factor equal to $(Y\pi f)\bigg/\left[\sqrt{2}\sqrt{\overline{v^2}}\,\sin\left(\pi f\,\frac{x}{u}\right)\right]$

r_C radius of curvature of deformed molecular-diffusion-wake center

S   stretched internodal length of molecular-diffusion-wake center

T   temperature, ^{O}R

ΔT temperature difference, $T - T_{am}$, ^{O}F

$\overline{\Delta T}$ time-mean temperature difference

t   residence time

U   stream velocity

u   axial velocity fluctuation

v   transverse velocity fluctuation, (i.e., particle velocity in sound wave)

X,Y   position of probe, or fixed point

x,y,z   Cartesian coordinates fixed in space

y   position of molecular-diffusion-wake center with respect to
                   flow axis plane

y_{max} maximum position of molecular-diffusion-wake center with
                   respect to flow axis plane = $(\sqrt{2} \sqrt{\overline{v^2}})/(\pi f)$

α coefficient of thermal diffusivity, $k/\rho c_p$

$\beta, \gamma, \varepsilon, \varkappa,$
λ, φ, ν variables of integration

Γ Gamma function

δ temperature fluctuation

ξ, η, ζ Cartesian coordinates moving with the stream

θ an angle

ρ density

σ thermal coefficient of resistance

τ time associated with the standing sound wave

ψ angle of X-wire array to stream direction

Ω electric resistance

ω molecular spreading coefficient

ω_x molecular spreading coefficient evaluated at X/U

Subscripts:

A   amplifier input

am   ambient

c   compensator

f   gas film

i   summation convention

L   electric cables

max   maximum

min   minimum

o   output

w   referring to hot wire

O   reference

1   any particular value for the variable

Superscript:

—   mean

APPENDIX B

DERIVATION OF EQUATIONS APPEARING IN THEORETICAL ANALYSIS

Approximate Analytic Solution of Exact

Instantaneous-Temperature Model

Equation (17) can be solved analytically for the special conditions:

$$\pi f t - \pi f \frac{X}{U} < 0.02 \ \pi f \frac{X}{U} \tag{B1}$$

$$f \frac{X}{U} = 4.5, \ 5.5, \ 6.5 \ . \ . \ . \tag{B2}$$

$$Y = 0 \tag{B3}$$

$$f \tau = 0.25, \ 0.75, \ 1.25 \ . \ . \ . \tag{B4}$$

$$\frac{U^2}{4\pi^2 f^2 \omega_X} \left(1 + \frac{\overline{2v^2}}{U^2}\right) > 50 \tag{B5}$$

Letting $\beta = \pi f t - \pi f \frac{X}{U}$ and using equation (13) for y in equation (16), result in

$$h = \frac{q/l}{4\pi\alpha} \int_{-\pi f \frac{X}{U}}^{\infty} \frac{1}{\left(\pi f \frac{X}{U} + \beta\right)} e^{-\frac{U^2}{4\pi\alpha f \left(\pi f \frac{X}{U} + \beta\right)} \left\{\beta^2 + \frac{\overline{2v^2}}{4U^2} \left[\cos(2\pi f\tau) - \cos\left(2\pi f\tau + 2\pi f \frac{X}{U} + 2\beta\right) - \frac{2Y}{y_{max}}\right]^2\right\}} \, d\beta \tag{B6}$$

It should be noted here that the application of condition (B1) limits the range of integration to the major values of the integrand. With conditions (B1), (B3), and (B4), an approximate form is

$$h \approx \frac{q/l}{4\pi^2 f \omega_X} \int_{-\pi f \frac{X}{U}}^{\infty} e^{-\frac{U^2}{4\pi^2 f^2 \omega_X} \left\{\beta^2 + \frac{\overline{2v^2}}{4U^2} \left[- \cos\left(2\pi f\tau + 2\pi f \frac{X}{U} + 2\beta\right)\right]^2\right\}} \, d\beta \tag{B7}$$

By trignometric identity and conditions (B2) and (B4),

$$
h \approx \frac{q/l}{4\pi^2 f \omega_X} \int_{-\pi f \frac{X}{U}}^{\infty} e^{-\frac{U^2}{4\pi^2 f^2 \omega_X}\left[\beta^2 + \frac{2\overline{v^2}}{4U^2}\left(\pm \sin 2\beta\right)^2\right]} d\beta \tag{B8}
$$

If the angle β is limited to the conditions

$$
|\beta| < 0.25 \tag{B9}
$$

then the sine of 2β can be replaced by 2β:

$$
h \approx \frac{q/l}{4\pi^2 f \omega_X} \int_{-\pi f \frac{X}{U}}^{\infty} e^{-\frac{U^2}{4\pi^2 f^2 \omega_X}\left(1 + \frac{2\overline{v^2}}{U^2}\right)\beta^2} d\beta \tag{B10}
$$

The imposition of condition (B9) is justified by condition (B5), which drives the integrand to small values at the limits of condition (B9). By change of variable, equation (B10) may be written

$$
h \approx \frac{q/l}{4\pi^2 f \ \omega_X} \sqrt{\frac{4\pi^2 f^2 \omega_X}{U^2\left(1 + \frac{2\overline{v^2}}{U^2}\right)}} \ \frac{\sqrt{\pi}}{2}\left[\frac{2}{\sqrt{\pi}}\int_{0}^{\pi f \frac{X}{U}\sqrt{\frac{U^2}{4\pi^2 f^2 \omega_X}\left(1 + \frac{2\overline{v^2}}{2}\right)}} e^{-\lambda^2} d\lambda + \frac{2}{\sqrt{\pi}}\int_{0}^{\infty} e^{-\lambda^2} d\lambda\right]
$$

$$\tag{B11}$$

By conditions (B2) and (B5), and by algebraic reduction,

$$
h \approx \frac{q/l}{U\sqrt{4\pi\omega_X}} \ \frac{1}{\sqrt{1 + \frac{2\overline{v^2}}{U^2}}} \quad \text{(for conditions (B1) through (B5))} \tag{B12}
$$

Calculation of Stretching of Molecular-Diffusion Wake

The stretched length S of the molecular-diffusion wake between adjacent nodal points in the mixing region can be calculated from the equation

$$S = \int_0^{U/f} \left[1 + \left(\frac{dy}{dx} \right)^2 \right]^{1/2} dx \tag{B13}$$

The derivative dy/dx can be determined from equation (12) in the THEORETICAL ANALYSIS section, so that the stretched length is

$$S = \int_0^{U/f} \left[1 + \frac{2\overline{v^2}}{U^2} \sin^2 \left(2\pi f\tau + 2\pi f \frac{x}{U} \right) \right]^{1/2} dx \tag{B14}$$

Since $\sin^2\theta = \cos^2\left(\theta - \frac{\pi}{2}\right)$ and $\cos^2\theta = 1 - \sin^2\theta$, equation (B14) may be written

$$S = \left(1 + \frac{2\overline{v^2}}{U^2} \right)^{1/2} \int_0^{U/f} \left[1 - \left(\frac{1}{\frac{U^2}{2\overline{v^2}} + 1} \right) \sin^2 \left(2\pi f\tau + 2\pi f \frac{x}{U} - \frac{\pi}{2} \right) \right]^{1/2} dx \tag{B15}$$

By the change of independent variable $\varphi = 2\pi f\tau + 2\pi f \frac{x}{U} - \frac{\pi}{2}$, and by noting the periodicity of the integrand, equation (B15) becomes

$$S = \frac{2U}{\pi f} \left(1 + \frac{2\overline{v^2}}{U^2} \right)^{1/2} \int_0^{\pi/2} \left[1 - \left(\frac{1}{\frac{U^2}{2\overline{v^2}} + 1} \right) \sin^2\varphi \right]^{1/2} d\varphi \tag{B16}$$

The integral is the complete elliptic integral of the second kind;

$$\mathscr{E} \equiv \int_0^{\pi/2} \left[1 - \left(\frac{1}{\frac{U^2}{2\overline{v^2}} + 1} \right) \sin^2\varphi \right]^{1/2} d\varphi \tag{B17}$$

so that the stretched length between adjacent nodal points is

$$S = \frac{2U}{\pi f}\left(1 + \frac{2\overline{v^2}}{U^2}\right)^{1/2} \mathscr{E} \tag{B18}$$

From equation (B18) a stretching parameter may be written

$$\frac{S - (U/f)}{(U/f)} = \frac{2}{\pi}\left(1 + \frac{2\overline{v^2}}{U^2}\right)^{1/2} \mathscr{E} - 1 \tag{B19}$$

Calculation of Radius of Curvature of Deformed

Molecular-Diffusion Wake

The formula for radius of curvature is

$$r_C = \frac{\left[1 + \left(\dfrac{dy}{dx}\right)^2\right]^{3/2}}{\left(\dfrac{d^2y}{dx^2}\right)} \tag{B20}$$

Taking the first and second derivatives of equation (11) and substituting into equation (B20) result in

$$r_C = \frac{\left[1 + \dfrac{2\overline{v^2}}{U^2}\sin^2\!\left(2\pi f\tau + 2\pi f\,\dfrac{x}{U}\right)\right]^{3/2}}{\dfrac{2\sqrt{2}\,\pi f\sqrt{\overline{v^2}}}{U^2}\left|\cos\!\left(2\pi f\tau + 2\pi f\,\dfrac{x}{U}\right)\right|} \tag{B21}$$

where the vertical bars indicate absolute values. The minimum radius of curvature $r_{C,\min}$ occurs when $2\pi f\tau + 2\pi f\,\frac{x}{U} = \pi, 2\pi, 3\pi, \ldots$, and its value is

$$r_{C,\min} = \frac{U^2}{2\sqrt{2}\,\pi f\sqrt{\overline{v^2}}} \tag{B22}$$

Approximate Solutions of Mean-Temperature Integral

for Negligible Wake Deformation

As shown in the THEORETICAL ANALYSIS section, an expression for the mean temperature $\overline{\Delta T}$ at any point in the mixing region is the integral equation formed from equations (29) and (30):

$$\overline{\Delta T} = f\, \Delta T_0 \int_0^{1/f} e^{-\frac{\overline{v^2}}{2\pi^2 f^2 \omega}\left[\sin\left(\frac{\pi f X}{U}\right)\sin\left(2\pi f \tau + \frac{\pi f X}{U}\right) - \frac{Y}{y_{max}}\right]^2} d\tau$$

(B23)

where

$$y_{max} = \left(\sqrt{2}\,\sqrt{\overline{v^2}}\right)/(\pi f)$$

Although an analytic solution could not be found for equation (B23), approximate solutions were found for the two regions shown in the following diagram:
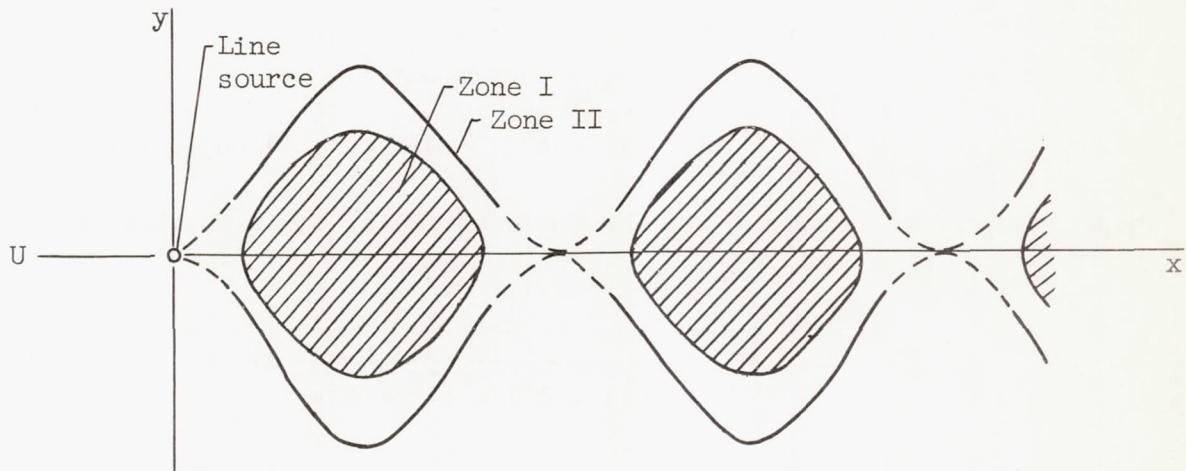
The conditions for approximate solutions in these two zones are:

	Y	x
Zone I	$Y < \dfrac{\sqrt{2}\sqrt{\overline{v^2}}}{\pi f}\sin\left(\pi f\,\dfrac{x}{U}\right)$	$0 < \dfrac{fX}{U} < 1 < \dfrac{fX}{U} < 2 \,\ldots$
Zone II	$Y = \dfrac{\sqrt{2}\sqrt{\overline{v^2}}}{\pi f}\sin\left(\pi f\,\dfrac{x}{U}\right)$	$0 < \dfrac{fX}{U} < 1 < \dfrac{fX}{U} < 2 \,\ldots$

Approximate solution for zone I. - By a change of variable, equation (B23) may be transformed to

$$\overline{\Delta T} = \frac{\Delta T_0}{2\pi} \int_{\pi f \frac{X}{U}}^{2\pi + \pi f \frac{X}{U}} e^{-F(\sin \varkappa - R)^2} \, d\varkappa \tag{B24}$$

where $\varkappa = 2\pi f \tau + \pi f \frac{X}{U}$, $F = \dfrac{\overline{v^2} \sin^2\left(\frac{\pi f X}{U}\right)}{2\pi^2 f^2 \omega}$, and $R = \dfrac{Y \pi f}{\sqrt{2}\sqrt{\overline{v^2}} \sin\left(\frac{\pi f X}{U}\right)}$.

Since the integral limits represent one cycle, equation (B24) may be written as

$$\overline{\Delta T} = \frac{\Delta T_0}{\pi} \int_{-\pi/2}^{\pi/2} e^{-F(\sin \varkappa - R)^2} \, d\varkappa \tag{B25}$$

By another change in variable, equation (B25) becomes

$$\overline{\Delta T} = \frac{\Delta T_0}{\pi} \int_{-1}^{1} \frac{e^{-F(\varepsilon - R)^2}}{\sqrt{1 - \varepsilon^2}} \, d\varepsilon \tag{B26}$$

where $\varepsilon = \sin \varkappa$. With a third change in variable, equation (B26) becomes

$$\overline{\Delta T} = \frac{\Delta T_0}{\pi} \int_{-1-R}^{1-R} \frac{e^{-F \nu^2}}{\sqrt{(1 - R^2) - (\nu^2 + 2R\nu)}} \, d\nu \tag{B27}$$

where $\nu = \varepsilon - R$. Expanding the integrand denominator in a binomial series in $(1 - R^2)$ and $(\nu^2 + 2R\nu)$, evaluating at the integral limits, and neglecting higher order terms give

$$\overline{\Delta T} \approx \frac{\Delta T_0}{2\sqrt{\pi F}\sqrt{1-R^2}} \left(\left[1 + \frac{1}{4F(1-R^2)}\right]\left\{ \operatorname{erf}\left[\sqrt{F}(1+R)\right] + \operatorname{erf}\left[\sqrt{F}(1-R)\right] \right\} - \right.$$

$$\left. \frac{1}{\sqrt{\pi F}(1 - R^2)}\left[\frac{1 - R}{2} e^{-F(1+R)^2} + \frac{1 + R}{2} e^{-F(1-R)^2} \right] \right) \tag{B28}$$

Noting that $\Delta T_0 = \dfrac{q/l}{\rho c_p U \sqrt{4\pi\omega}}$, equation (B28) may be further reduced to

$$\overline{\Delta T} \approx \frac{q/l}{2\sqrt{2}\rho c_p \sqrt{1-R^2}} \left[\frac{f}{\sqrt{v^2}U \left|\sin\left(\pi f \, \frac{X}{U}\right)\right|} \right] \left(\left[1 + \frac{1}{4F(1-R^2)}\right] \left\{ \mathrm{erf}\left[\sqrt{F}(1+R)\right] + \mathrm{erf}\left[\sqrt{F}(1-R)\right] \right\} - \right.$$

$$\left. \frac{1}{\sqrt{\pi}\,\sqrt{F}(1-R)} \left[\frac{1-R}{1+R} \, e^{-F(1+R)^2} + e^{-F(1-R)^2} \right] \right) \tag{B29}$$

Approximate solution for zone II. - When $Y = -\left(\dfrac{\sqrt{2}\sqrt{v^2}}{\pi f}\right)\sin\left(\pi f \, \dfrac{X}{U}\right)$, then $R = -1$, so that equation (B27) becomes

$$\overline{\Delta T} \approx \frac{\Delta T_0}{\pi} \int_0^2 \frac{e^{-Fv^2}}{\sqrt{2v - v^2}} \, dv \tag{B30}$$

Expanding the integrand denominator in a binomial series and neglecting higher order terms,

$$\overline{\Delta T} \approx \frac{\Delta T_0}{\pi} \int_0^2 \frac{e^{-Fv^2}}{\sqrt{2v}} \, dv \tag{B31}$$

By a change in variable, equation (B31) becomes

$$\overline{\Delta T} \approx \frac{\sqrt{2}}{F^{1/4}} \frac{\Delta T_0}{\pi} \int_0^{\sqrt{2}\,F^{1/4}} e^{-\gamma^4} \, d\gamma \tag{B32}$$

As shown in reference 8, when $\sqrt{2}\,F^{1/4} > 1$, equation (B32) is approximated by

$$\overline{\Delta T} \approx \frac{\sqrt{2}}{F^{0.25}} \frac{\Delta T_0}{\pi} \, \Gamma(1.25) \tag{B33}$$

Solution for Instantaneous Temperature for Small Wake

Deformation Allowing for Wake Curvature

The THEORETICAL ANALYSIS section presents two approximate solutions for small deformations of the molecular-diffusion wake. Figure 4 shows the geometric assumptions used in deriving these equations. In equation (26), the slope of the wake center plane was assumed constant over the small range of η which is of interest. Derivation of equation (27) assumed further that the slope was essentially zero, thereby making it possible to neglect the contribution of the axial displacement to η.

The following derivation considers the curvature of the wake center plane. The position of the wake at any particular fraction of a cycle $f\tau_1$ is given by

$$ y = \frac{\sqrt{2}\sqrt{v^2}}{\pi f} \sin\left(\frac{\pi f x}{U}\right) \sin\left(2\pi f \tau_1 + \frac{\pi f x}{U}\right) \qquad (B34) $$

There is a point (x_1, y_1) satisfying equation (B34) which is a minimal distance η from the probe at (X, Y). This minimal distance condition requires that η be measured normal to the center plane curve, as shown in figure 4. Therefore, the equation for the slope and end points of the line segment η must be given by

$$ \frac{y_1 - Y}{x_1 - X} = \frac{1}{-\left(\dfrac{dy}{dx}\right)_{x_1, y_1, \tau_1}} \qquad (B35) $$

where

$$ \frac{1}{\left(\dfrac{dy}{dx}\right)_{x_1, y_1, \tau_1}} = \frac{U}{\sqrt{2}\sqrt{v^2}} \frac{1}{\sin\left(2\pi f \tau_1 + \dfrac{2\pi f x_1}{U}\right)} \qquad (B36) $$

Combination of (B35) and (B36) gives

$$ y_1 - Y = \frac{U}{\sqrt{2}\sqrt{v^2}} \frac{(X - x_1)}{\sin\left(2\pi f \tau_1 + \dfrac{2\pi f x_1}{U}\right)} \qquad (B37) $$

Equations (B34) and (B37) define all that is needed to calculate the minimal distance η for any time τ_1. Direct substitution of η into

equations (9) and (2) gives the instantaneous temperature at any position within the mixing region. The actual procedure used to obtain figure 11 is outlined in the following paragraphs.

The solution of equations (B34) and (B37) simultaneously for x_1 is

$$\sin\left(2\pi f\tau_1 + \frac{\pi f x_1}{U}\right) - \frac{\pi f U}{2v^2} \frac{(X - x_1)}{\sin\left(\frac{\pi f x_1}{U}\right)\sin\left(2\pi f\tau_1 + \frac{2\pi f x_1}{U}\right)} - \frac{\pi f}{\sqrt{2}\sqrt{v^2}} \frac{Y}{\sin\left(\frac{\pi f x_1}{U}\right)} = 0 \tag{B38}$$

For assigned values of x_1 near the probe-position plane X, equation (B38) can be solved for $f\tau_1$ by successive trials. The corresponding value of y_1 is obtained from equation (B34), and the calculation of η at this particular $f\tau_1$ can be made using the following equation:

$$\eta_1 = \left[(X - x_1)^2 + (Y - y_1)^2\right]^{1/2} \tag{B39}$$

The subscript 1 indicates that the distance corresponds to a particular $f\tau_1$.

The instantaneous temperature ΔT_1 at this fraction of a cycle may be made by using the following simplification of equations (9) and (2):

$$\Delta T_1 = \Delta T_0 \, e^{-(\eta_1)^2/4\omega} \tag{B40}$$

where $\Delta T_0 = (q/l)/(\sqrt{4\pi\omega} \, \rho c_p U)$, and η_1 is given by equation (B39). Equation (B40) is restricted by the two conditions discussed in "Approximate model for small deformation of diffusion wake." If these conditions are satisfied, this analysis is a better approximation of the exact solution (eq. (17)) than either equations (28) or (29). However, it is obviously a far more tedious procedure.

APPENDIX C

FLOW AND SOUND-FIELD MEASUREMENTS

Stream Velocity

The stream velocity was measured by the vortex-shedding technique described in reference 9. The frequency of vortex shedding from a 0.250-inch-diameter cylinder was determined by forming a Lissajou's figure from a hot-wire anemometer signal. The stream velocity was then calculated from the frequency of shedding by means of the Strouhal number.

Stream Static Temperature and Pressure

The stream temperature was measured with a mercury thermometer at the calming-chamber inlet. The stream pressure was measured with a barometer and differential water manometer.

Transverse Velocity Fluctuation

The transverse velocity fluctuation v was measured with an X-wire anemometer. Since the velocity antinode and pressure-node planes of the standing sound wave passed through the line source and stream centerline, the velocity fluctuations were at a maximum and the pressure fluctuations were negligible in the mixing region. Since both turbulent velocity fluctuations and pressure fluctuations were negligible, the X-wire anemometer could be used to measure the transverse velocity fluctuation.

The operation and design of the X-wire anemometer equipment has been described in references 1 and 10, and will be only outlined here. The X-wire probe and circuit diagram were identical to those described in reference 10. The sensitivity of the X-wire is given by the equation

$$v = \frac{U}{G(\Delta E/\Delta \psi)}\, e \tag{C1}$$

where e is the alternating-voltage difference between the two hot wires, G is the amplifier gain, and $\Delta E/\Delta \psi$ is the slope of the X-wire calibration curve. A typical plot of the direct-current-voltage difference between the hot wires E and the relative angle between the X-array and the stream direction ψ is shown in reference 1.

The root-mean-square value of the transverse velocity fluctuation $\sqrt{\overline{v^2}}$ was measured with a true root-mean-square voltmeter. The sound-wave velocity $v(\tau)$ was also recorded in the form of oscillograms.

APPENDIX D

INSTANTANEOUS-TEMPERATURE MEASUREMENTS WITH RESISTANCE THERMOMETER

A standard single-wire anemometer probe was used as the sensitive element of the resistance-thermometer equipment and is shown in figure 13(a). The resistance thermometer circuit design was based on unpublished instrument research by Mr. E. Carlson of the Lewis laboratory. The circuit diagram for the resistance thermometer is shown in figure 13(b). With the "run-calibrate switch" in the calibrate position, a step-function current could be impressed on the resistance thermometer. A typical time response of the resistance element to this step-current is shown in figure 14(a). Since the resistance element was known to have an exponential response curve, its time constant could be measured directly from oscillograms as shown in figure 14(b).

With the "run-calibrate switch" in the run position, the circuit in figure 13(b) could be used as a compensated resistance thermometer. The sensitivity of the instrument to temperature fluctuations is given by the expression

$$\delta = \frac{T_{am}\left[0.1404(\Omega_{am} + \Omega_L) + 1\right] e}{31.62 \ GG_c I_w \Omega_{am}\left[\dfrac{\sigma T_{am}}{1 + \sigma(T_{am} - T_0)}\right]} \tag{D1}$$

where δ is the temperature fluctuation, T_{am} is the ambient air temperature, Ω_{am} is the wire resistance at the temperature T_{am}, Ω_L is the probe lead resistance, G is the gain of the amplifier, I_w is the wire current, σ is the thermal coefficient of resistance of the wire material, e is the amplifier output voltage, and 31.62 G_c is the gain of the resistance thermometer circuit where G_c is given by the expression

$$G_c = \sqrt{\frac{1}{\dfrac{\Omega_c}{\Omega_0}\left(\dfrac{\Omega_c}{\Omega_0} + 2\right)\left(1 + \dfrac{\Omega_0}{\Omega_A}\right) + 1 + (2\pi f \Omega_c C)^2}} \tag{D2}$$

In the present experiment, the circuit components were adjusted so that the term $(2\pi f \Omega_c C)^2$ was small compared to the first term in the denominator. The gain G_c could then be approximated by the expression

$$G_c = \sqrt{\dfrac{1}{\dfrac{\Omega_c}{\Omega_0}\left(\dfrac{\Omega_c}{\Omega_0} + 2\right)\left(1 + \dfrac{\Omega_0}{\Omega_A}\right) + 1}} \tag{D3}$$

In operation, the time constant M was determined from an oscillogram of the time response of the resistance element to the step current. The resistances Ω_c and Ω_0 were then adjusted so that

$$\Omega_c C = M \tag{D4}$$

and

$$\frac{\Omega_c}{\Omega_0} = 14 \tag{D5}$$

With the condition (D5), the over-all circuit frequency response was flat within 3 percent from 20 to 500 cycles per second. With the correct compensation, the circuit was then used to obtain oscillograms of the instantaneous-temperature fluctuation at a number of points in the mixing region.

APPENDIX E

INSTANTANEOUS-TEMPERATURE MEASUREMENTS WITH HOT-WIRE ANEMOMETER

As pointed out in reference 11, the hot-wire anemometer theoretically can be used to measure temperature fluctuations simultaneously with velocity fluctuations. In the present experiment, the axial velocity fluctuations were negligible, so that a single hot wire placed normal to the flow direction should be sensitive only to temperature fluctuations. However, for clarity and future reference, the hot-wire sensitivity equation is derived herein for both temperature and velocity fluctuations. The derivation is made for constant-temperature operation of the hot wire.

Derivation of Sensitivity Equation

In reference 11, King's equation is written:

$$I^2 \Omega = (A + B \sqrt{U})(\Omega - \Omega_{am}) \tag{E1}$$

where I and Ω are the hot-wire current and operating resistance, respectively. The factors A and B and the cold-wire resistance Ω_{am} are functions of temperature as follows:

$$A = \frac{a l}{\Omega_0 \sigma} k \tag{E2}$$

$$B = \frac{b l}{\Omega_0 \sigma} \sqrt{\mathscr{D} c_p \rho k} \tag{E3}$$

$$\Omega_{am} = \Omega_0 \left[1 + \sigma(T_{am} - T_0) \right] \tag{E4}$$

where a and b are constants, l is the wire length, $\mathscr{D}$ is the wire diameter, σ is the thermal coefficient of resistance of the wire material, Ω_0 is the wire resistance at the reference temperature T_0, Ω_{am} is the wire resistance at the ambient temperature T_{am}, k is the fluid thermal conductivity, c_p is the fluid isobaric specific heat, and ρ is the fluid density.

In the temperature range from 500° to 1000° R, the thermal conductivity of air is closely approximated by

$$k = f T_{am}^{0.851} \tag{E5}$$

where f is a constant, and the exponent 0.851 was evaluated from the data of reference 12. Since the specific heat c_p has negligible change in the temperature range 500° to 1000° R, equations (E2) and (E3) can be written as

$$A = \left(\frac{a l f}{\Omega_0 \sigma}\right) \left[T - m(T - T_{am})\right]^{0.851} \tag{E6}$$

$$B = \left(\frac{b l}{\Omega_0 \sigma} \sqrt{\mathscr{D} c_p f g}\right) \left[T - m(T - T_{am})\right]^{-0.0745} \tag{E7}$$

where $\left[T - m(T - T_{am})\right]$ is the film temperature appropriate to the heat transfer from the hot wire at temperature T to the fluid stream at temperature T_{am} and m is an unknown constant.

With A, B, and Ω_{am} given in terms of the temperature T_{am}, equation (E1) can be differentiated to obtain the combined temperature and velocity sensitivity of a constant-temperature hot-wire anemometer (Ω, and therefore T, held constant):

$$2I\Omega \, dI = \frac{\partial}{\partial T_{am}} \left[(A + B\sqrt{U})(\Omega - \Omega_{am})\right] dT_{am} + \frac{\partial}{\partial U} \left[(A + B\sqrt{U})(\Omega - \Omega_{am})\right] dU \tag{E8}$$

By noting that the voltage fluctuation across the hot wire is $e = \Omega dI$ and defining the temperature and velocity fluctuations as $\delta = dT_{am}$ and $u = dU$, respectively, equation (E8) becomes

$$2Ie = \left[(A + B\sqrt{U}) \frac{\partial}{\partial T_{am}} (\Omega - \Omega_{am}) + \right.$$

$$\left. (\Omega - \Omega_{am}) \left(\frac{\partial A}{\partial T_{am}} + \sqrt{U} \frac{\partial B}{\partial T_{am}}\right)\right] \delta + \left[\frac{(\Omega - \Omega_{am}) B_1}{2\sqrt{U}}\right] u \tag{E9}$$

The various partial derivatives are

$$\frac{\partial}{\partial T_{am}} (\Omega - \Omega_{am}) = -\sigma\Omega_0 = - \frac{\sigma\Omega_a}{1 + \sigma(T_{am} - T_0)} \tag{E10}$$

$$\frac{\partial A}{\partial T_{am}} = \left(\frac{alf}{\Omega_0 \sigma}\right)(0.851 \text{ m})\left[T - m(T - T_{am})\right]^{-0.149} = \frac{0.851 \text{ m}\overline{A}}{\left[T - m(T - T_{am})\right]}$$

(E11)

$$\frac{\partial B}{\partial T_{am}} = -\frac{0.0745 \text{ m}\overline{B}}{\left[T - m(T - T_{am})\right]}$$

(E12)

By assuming negligible natural-convection effects, the mean values $\overline{A}$ and $\overline{B}$ can be written as

$$\overline{A} = \frac{I_0^2 \Omega}{\Omega - \Omega_{am}}$$

(E13)

$$\overline{B} = \frac{(I^2 - I_0^2)}{\sqrt{U}(\Omega - \Omega_{am})}$$

(E14)

where I_0 is the wire current at the stream temperature and pressure, but with zero velocity.

Substitution of equations (E10) through (E14) into equation (E9) results in the desired sensitivity equation

$$e = \frac{I\Omega}{2T_{am}} \left\{ -\frac{\Omega_{am}}{\Omega - \Omega_{am}} \left[\frac{\sigma T_{am}}{1 + \sigma(T_{am} - T_0)}\right] + \left[\frac{1}{\frac{T}{T_{am}}\left(\frac{1}{m} - 1\right) + 1}\right]\left[0.925\left(\frac{I_0}{I}\right)^2 - 0.0745\right] \right\} \delta + \frac{I\Omega}{4U}\left[1 - \left(\frac{I_0}{I}\right)^2\right]u$$

(E15)

Hot-Wire-Anemometer Circuitry and Operation

The hot-wire-anemometer probe used for the temperature fluctuation measurements is shown in figure 15(a), and the circuit diagram was the same as that used in reference 10. Since the velocity fluctuations in the axial direction had negligible effect on a single hot wire positioned normal to the stream direction, equation (E15) could be modified to relate the oscilloscope display voltage to the stream temperature fluctuations as follows:

$$\delta = \cfrac{2T_{am}e_o}{I\Omega(2G)\left\{-\cfrac{\Omega_{am}}{\Omega-\Omega_{am}}\left[\cfrac{\sigma T_{am}}{1+\sigma(T_{am}-T_0)}\right]+\left[\cfrac{1}{\cfrac{T}{T_{am}}\left(\cfrac{1}{m}-1\right)+1}\right]\left[0.925\left(\cfrac{I_0}{I}\right)^2-0.0745\right]\right\}}$$

$$(E16)$$

where $2G$ is the gain of the bridge-amplifier combination, and e_o is the voltage displayed on the oscilloscope.

Hot-Wire-Anemometer Measurements

The sinusoidal wave to be seen at the base of the hot-wire-anemometer oscillograms in figure 7(a) is due to the influence of the transverse velocity fluctuation v on the hot-wire heat loss. As shown above, the sensitivity of the hot-wire anemometer to temperature fluctuations depends on the film temperature $T_f = T_W - m(T_W - T_{am})$. When the constant m is set equal to 1.0 (so that $T_f = T_{am}$), and when the oscillograms are corrected for the effect of v, then the peak temperature difference ΔT_0 measured by hot-wire anemometry shows good agreement with the peak temperature ΔT_0 predicted by equation (7). The equivalence of T_f and T_{am} is in agreement with previous results reported in reference 13, where the term A (eq. (E2)) was found to be a function of the ambient fluid temperature.

In summary, the hot-wire-anemometer measurements substantiate those of the resistance thermometer when the film temperature was taken equal to the ambient temperature. Further research is necessary before the equivalence of film and ambient temperature is fully established.

APPENDIX F

MEAN-TEMPERATURE MEASUREMENTS

The mean-temperature measurements were made with an iron-constantan thermopile probe shown in figure 15(a). The thermojunctions were carefully alined to fall on a line parallel to the line source of heat. The circuit diagram is shown in figure 15(b). The time constant of the thermocouples was high enough to ensure true averaging of temperature fluctuations, so that the emf read with the potentiometer was in direct proportion to the mean temperature difference $\overline{\Delta T}$.

REFERENCES

1. Mickelsen, William R., and Laurence, James C.: Measurement and Analysis of Turbulent Flow Containing Periodic Flow Fluctuations. NACA RM E53F19, 1953.

2. Blackshear, Perry L., Rayle, Warren D., and Tower, Leonard K.: Study of Screeching Combustion in a 6-Inch Simulated Afterburner. NACA TN 3567, 1955.

3. Corrsin, Stanley, and Uberoi, Mahinder S.: Further Experiments on the Flow and Heat Transfer in a Heated Turbulent Air Jet. NACA Rep. 998, 1950. (Supersedes NACA TN 1865.)

4. Townsend, A. A.: The Diffusion Behind a Line Source in Homogeneous Turbulence. Proc. Roy. Soc. (London), ser. A, vol. 224, no. 1159, July 22, 1954, pp. 487-512.

5. Drew, Thomas Bradford: Mathematical Attacks on Forced Convection Problems: A Review. Trans. Am. Inst. Chem. Eng., vol. 26, 1931, pp. 26-80.

6. Jakob, Max: Heat Transfer. Vol. I. John Wiley & Sons, 1949, p. 340.

7. Frenkiel, F. N.: Turbulent Diffusion: Mean Concentration Distribution in a Flow Field of Homogeneous Turbulence. Vol. III. Advances in Appl. Mech., Academic Press, Inc., 1953, pp. 61-107.

8. Jahnke, Eugen, and Emde, Fritz: Tables of Functions. Fourth ed., Dover Pub., 1945, p. 23.

9. Roshko, Anatol: On the Development of Turbulent Wakes from Vortex Streets. NACA Rep. 1191, 1954. (Supersedes NACA TN 2913.)

10. Mickelsen, William R.: An Experimental Comparison of the Lagrangian and Eulerian Correlation Coefficients in Homogeneous Isotropic Turbulence. NACA TN 3570, 1955.

11. Corrsin, Stanley: Extended Applications of the Hot-Wire Anemometer. NACA TN 1864, 1949.

12. Hilsenrath, Joseph, et al.: Tables of Thermal Properties of Gases. Circular 564, U.S. Dept. Commerce, Nat. Bur. Standards, Nov. 1, 1955.

13. Corrsin, Stanley, and Uberoi, Mahinder S.: Spectra and Diffusion in a Round Turbulent Jet. NACA Rep. 1040, 1951. (Supersedes NACA TN 2124.)
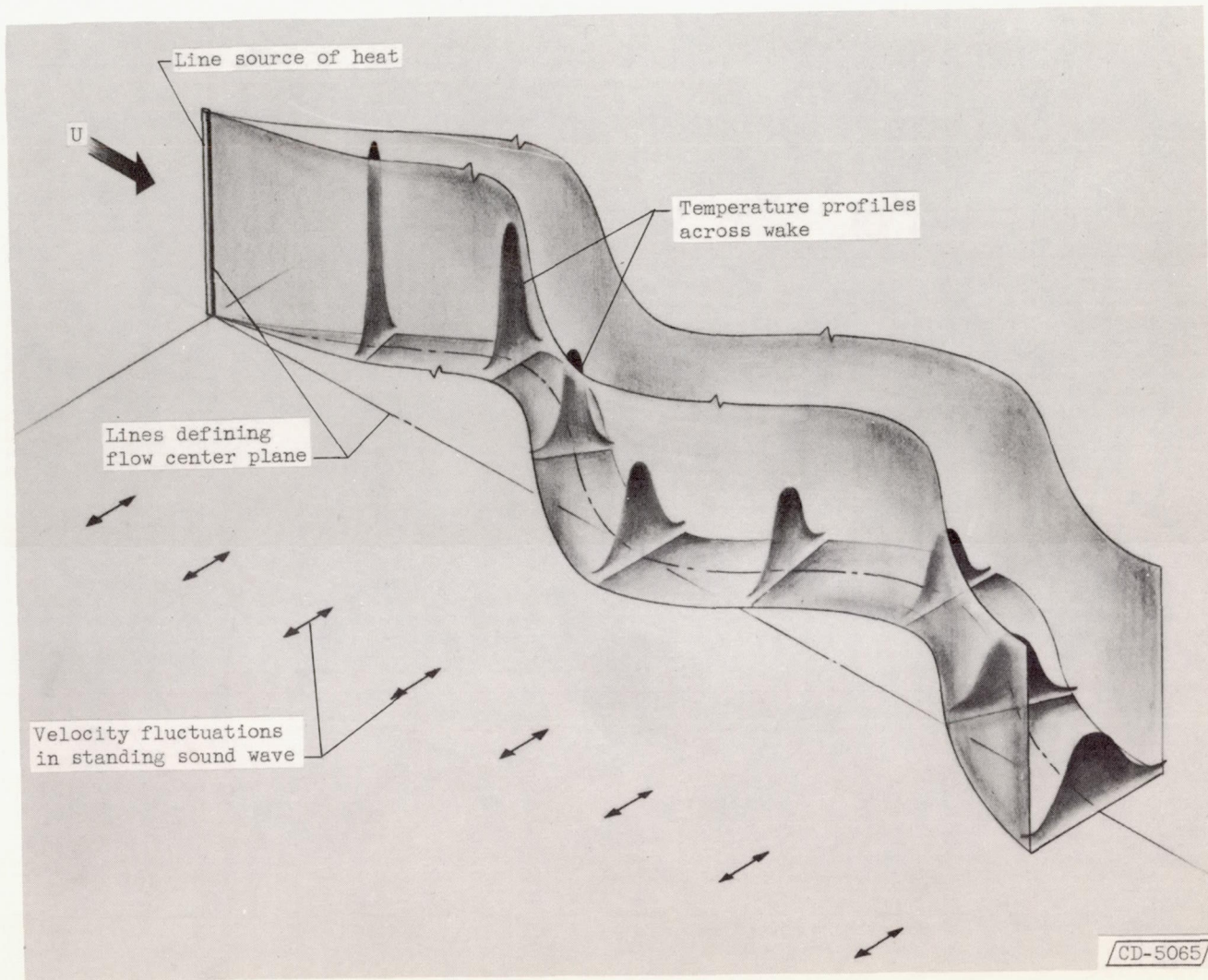
(a) Typical temperature profiles in molecular-diffusion wake at an instant.

Figure 1. - Position of molecular-diffusion wake in mixing region.
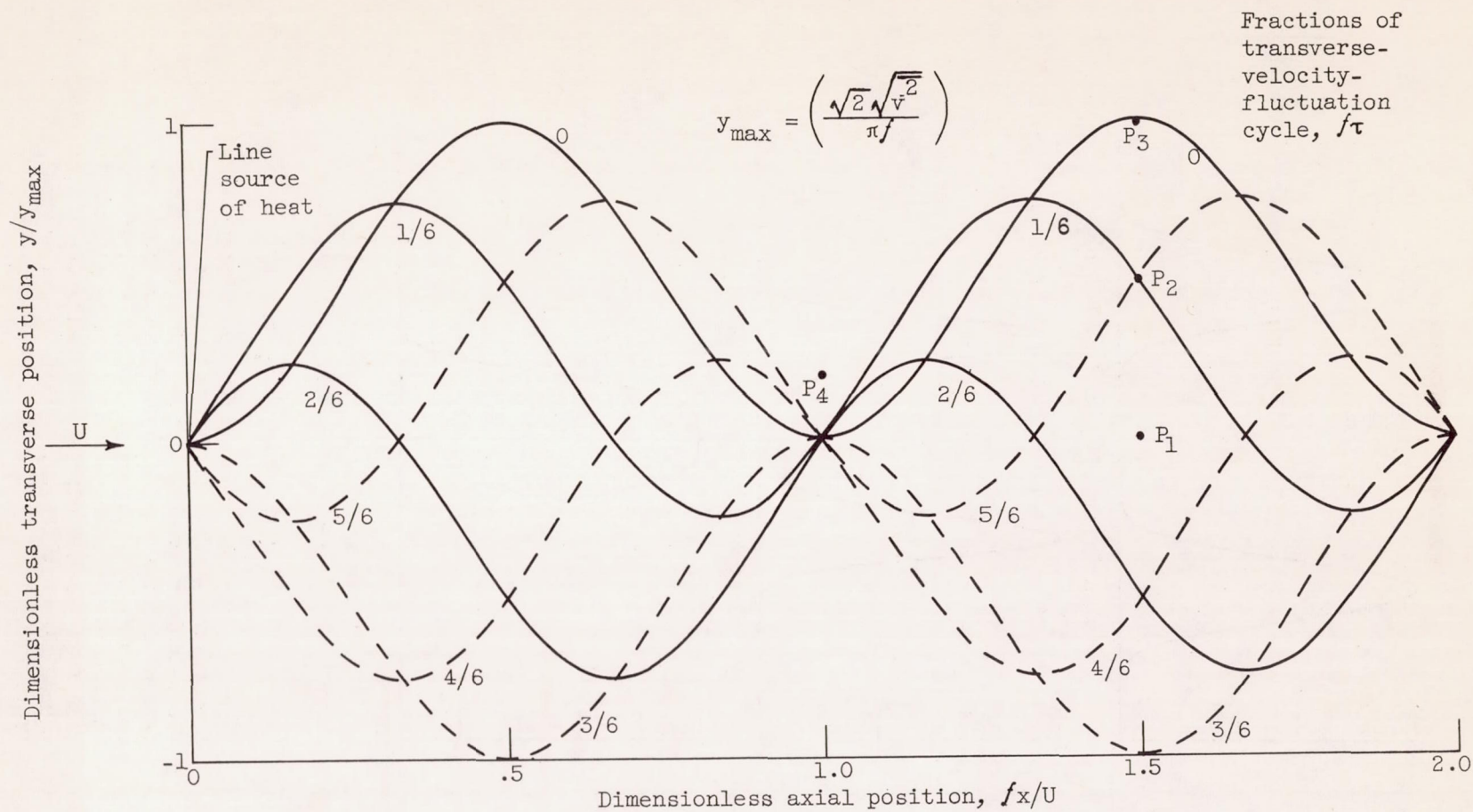
(b) Position of molecular-diffusion-wake center at various times through one cycle of transverse-velocity fluctuation.

Figure 1. - Concluded. Position of molecular-diffusion wake in mixing region.

(a) At point P_1 in figure 1(b).

(b) At point P_2 in figure 1(b).

Fractions of transverse-velocity-
fluctuation cycle, $f\tau$

(c) At point P_3 in figure 1(b).
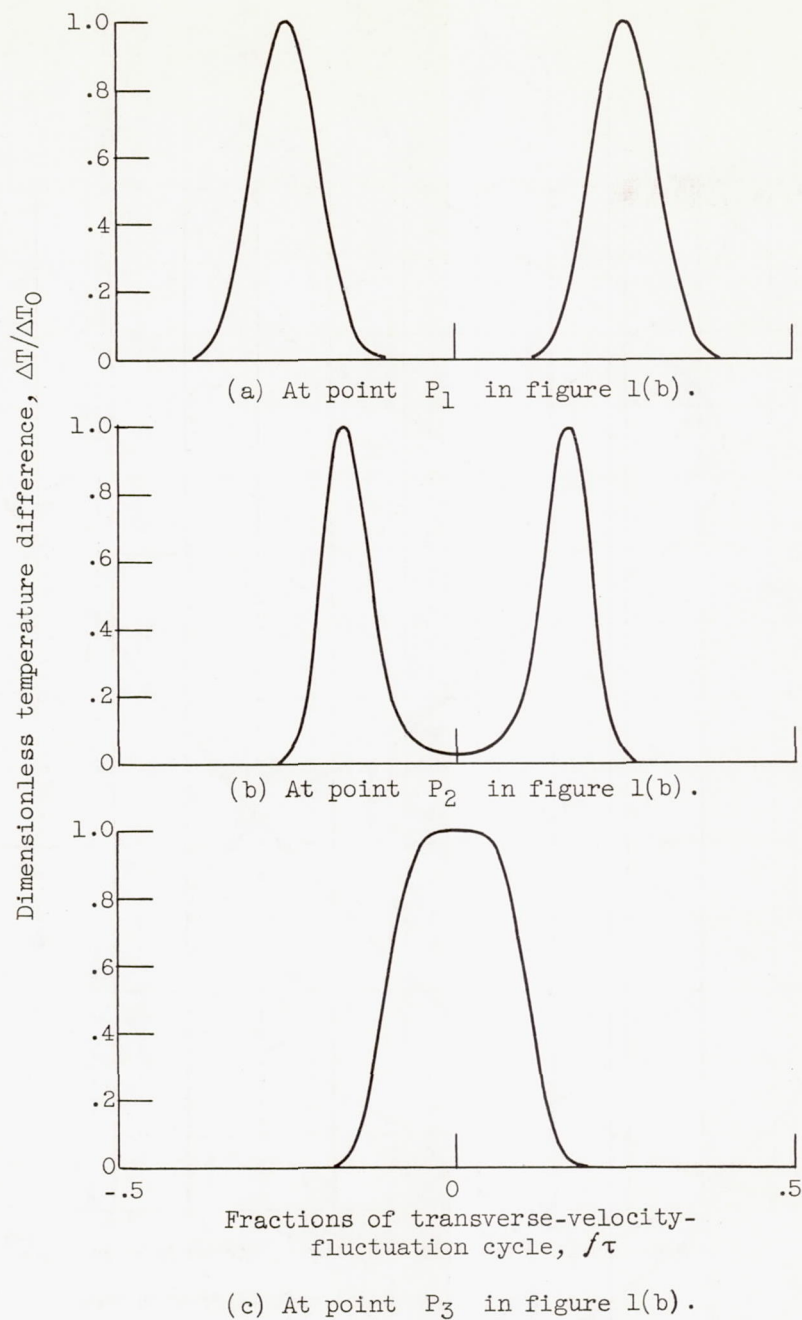
Figure 2. - Typical theoretical instantaneous-
temperature - time variations in mixing region.
Dimensionless axial position, 1.5; coefficient of
thermal diffusivity, 2.37×10^{-4} square feet per sec-
ond; sound-wave frequency, 104 cycles per second;
root-mean-square transverse velocity fluctuation,
3.33 feet per second; rate of heat release from line
source per unit length, 0.0308 Btu per second per
foot.
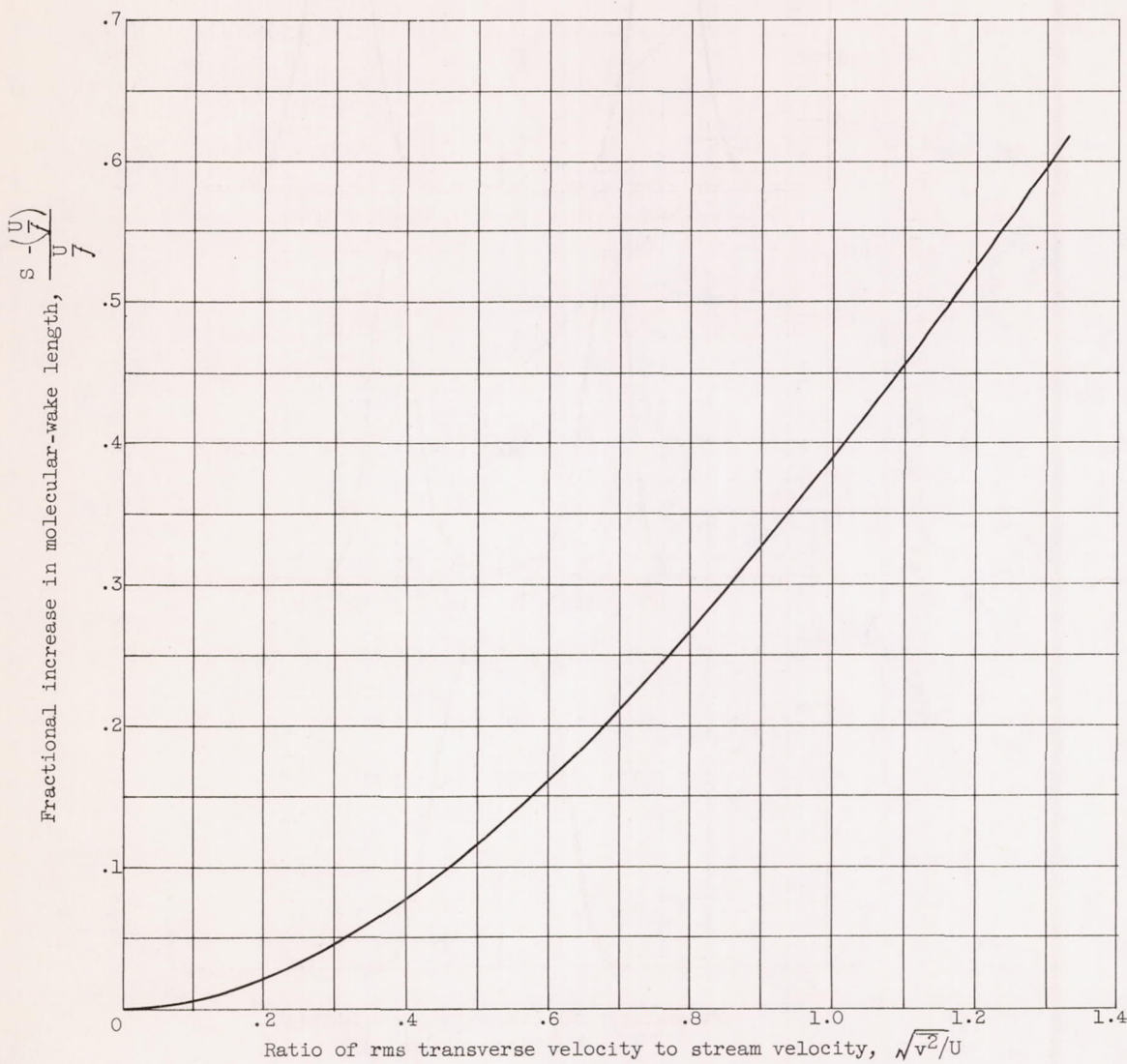
(a) Stretching of molecular-diffusion wake.

Figure 3. - Factors characterizing deformation of molecular-diffusion wake.
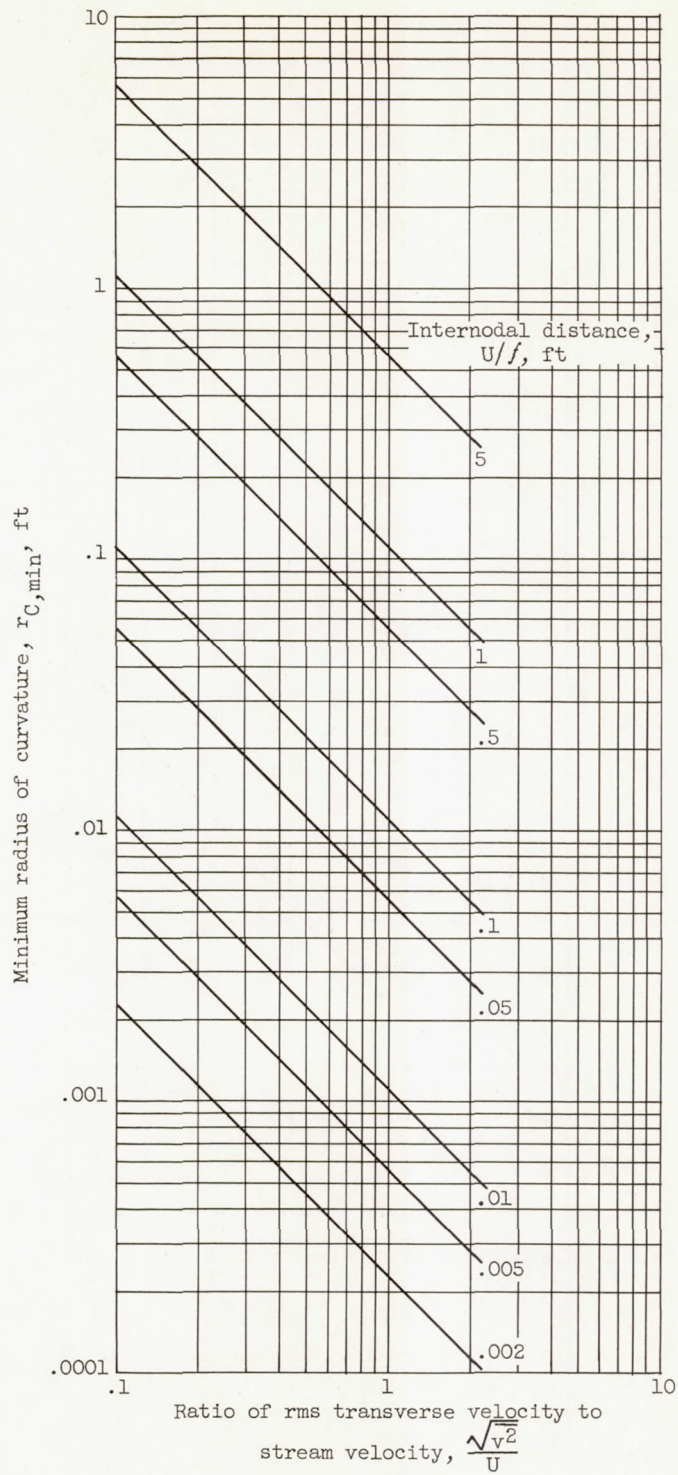
(b) Minimum radius of curvature of molecular-
diffusion wake.

Figure 3. - Continued. Factors characterizing
deformation of molecular-diffusion wake.
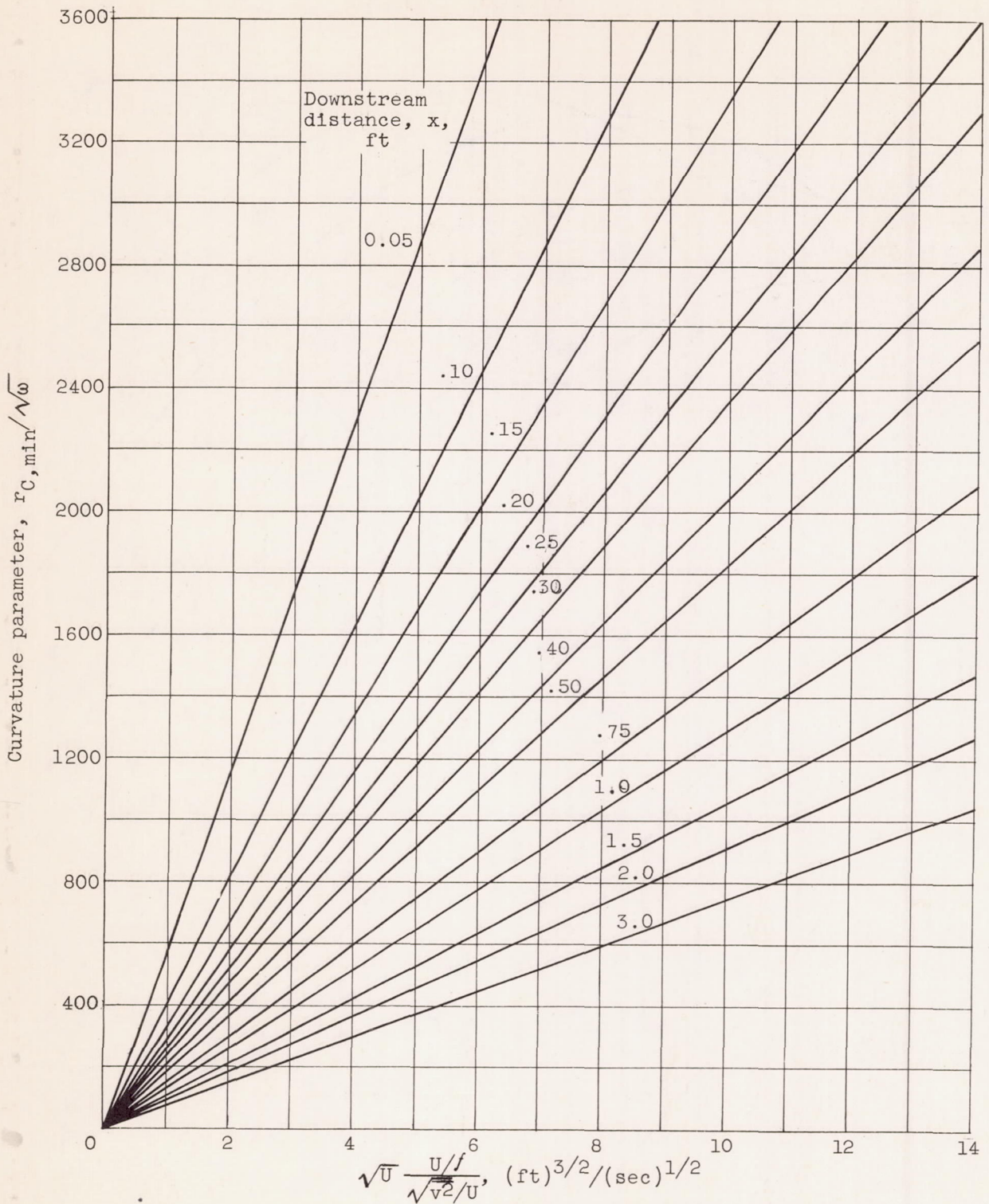
(c) Curvature parameter; coefficient of thermal diffusivity, 2.37×10^{-4} square feet per second.

Figure 3. - Concluded. Factors characterizing deformation of molecular-diffusion wake.
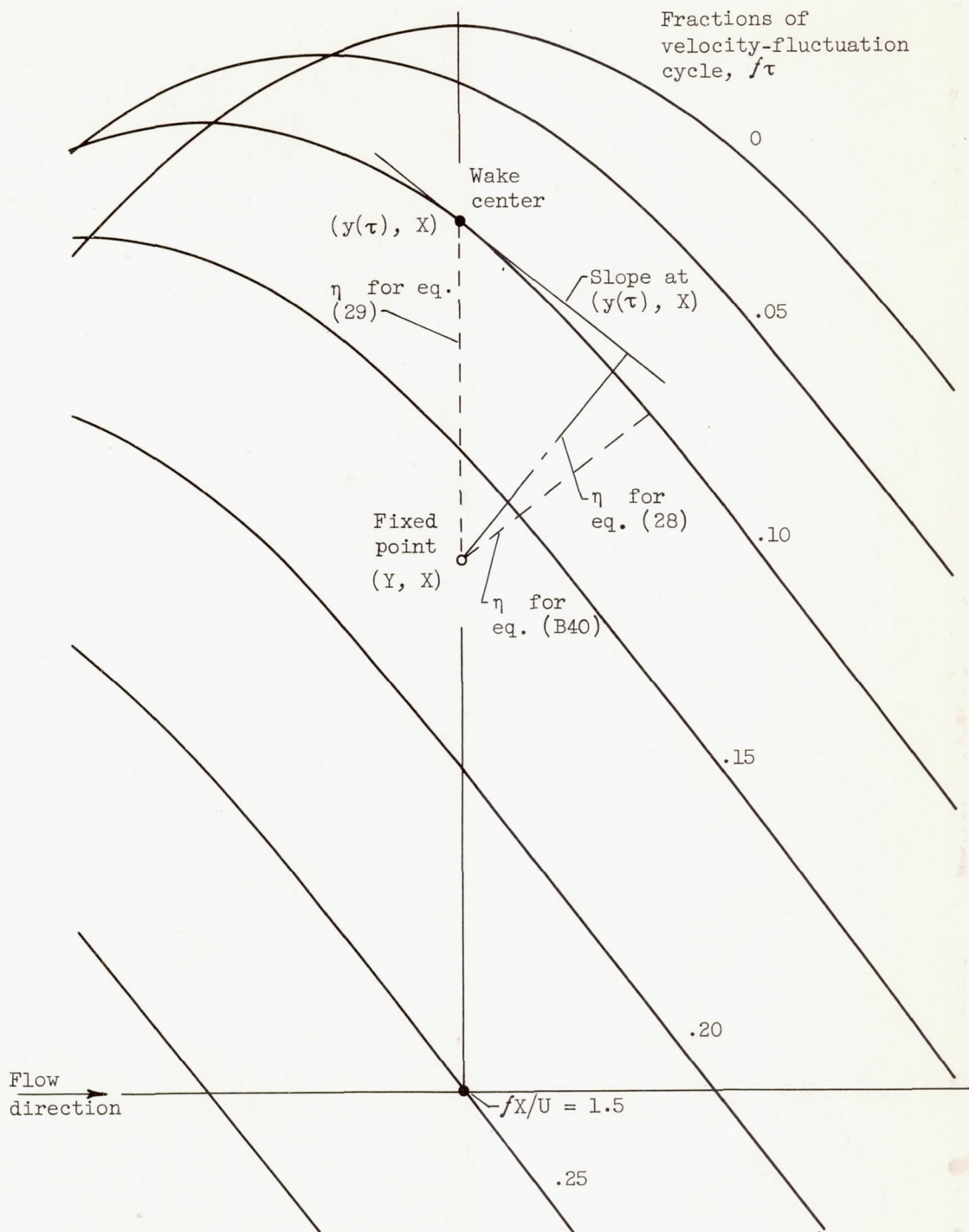
Figure 4. - Local diagram of position of molecular-diffusion-wake
center at various times.
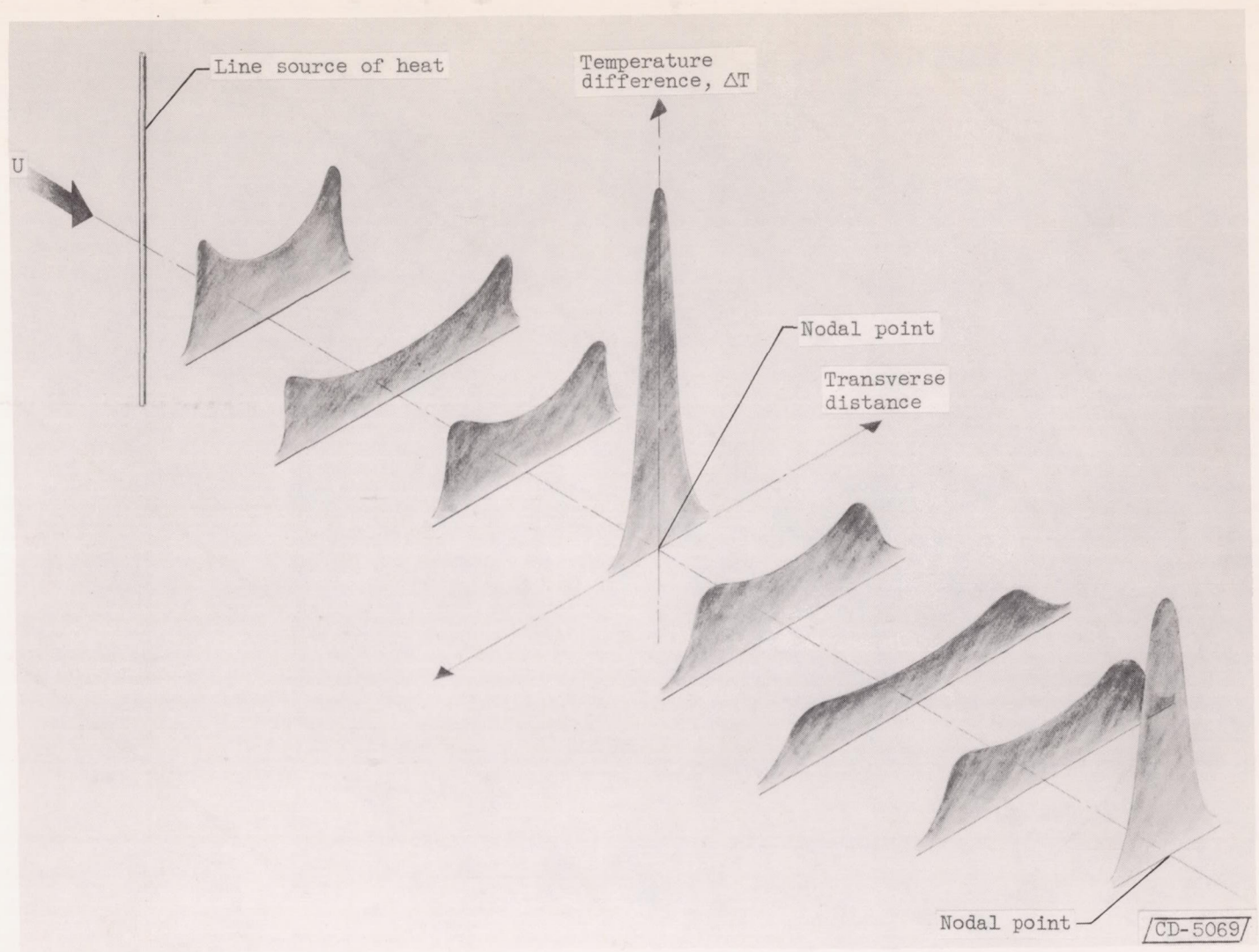
Figure 5. - Typical time-mean temperature profiles in mixing region for small deformation of the molecular-diffusion wake.
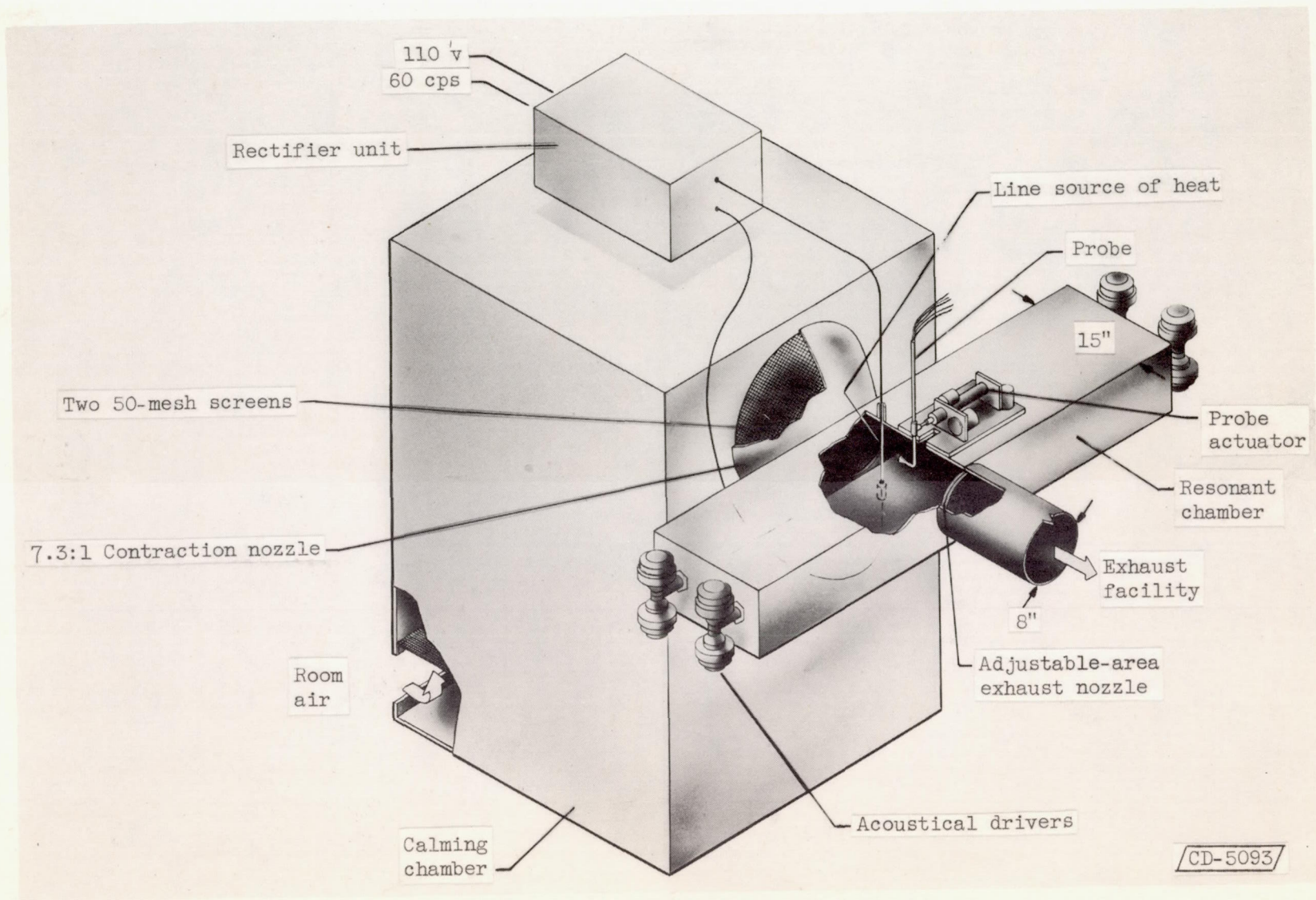
Figure 6. - Flow and sound-field apparatus.
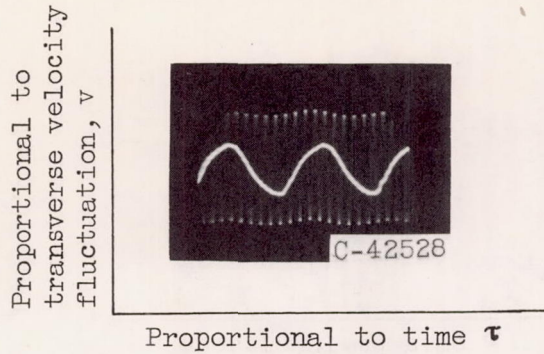
(a) Typical oscillogram of transverse velocity fluctuation.
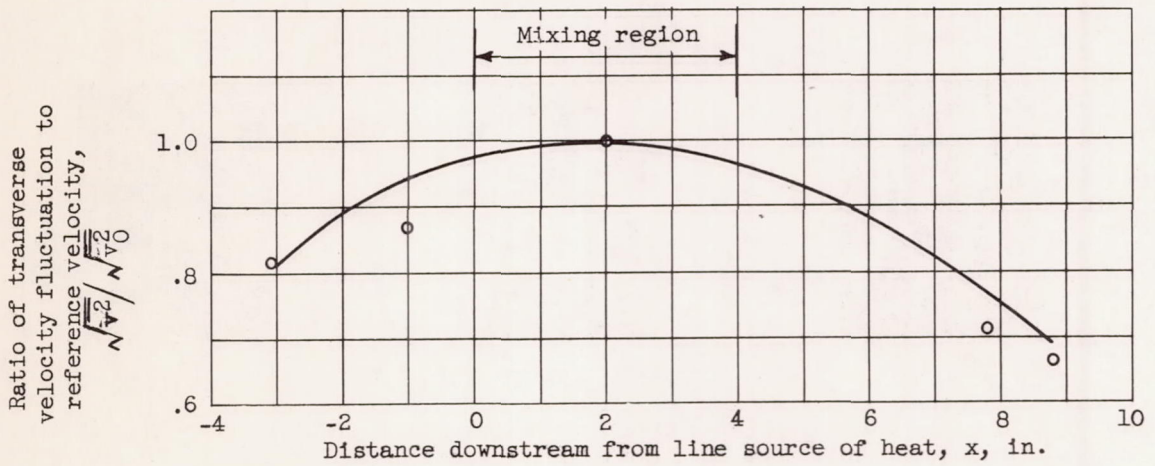
(b) Axial profile of velocity fluctuation in transverse standing sound wave. Reference root-mean-square transverse velocity fluctuation at x = 2 inches.

Figure 7. - Transverse-velocity-fluctuation data.

(a) Hot-wire-anemometer data.

Proportional to time τ

(b) Resistance-thermometer data.
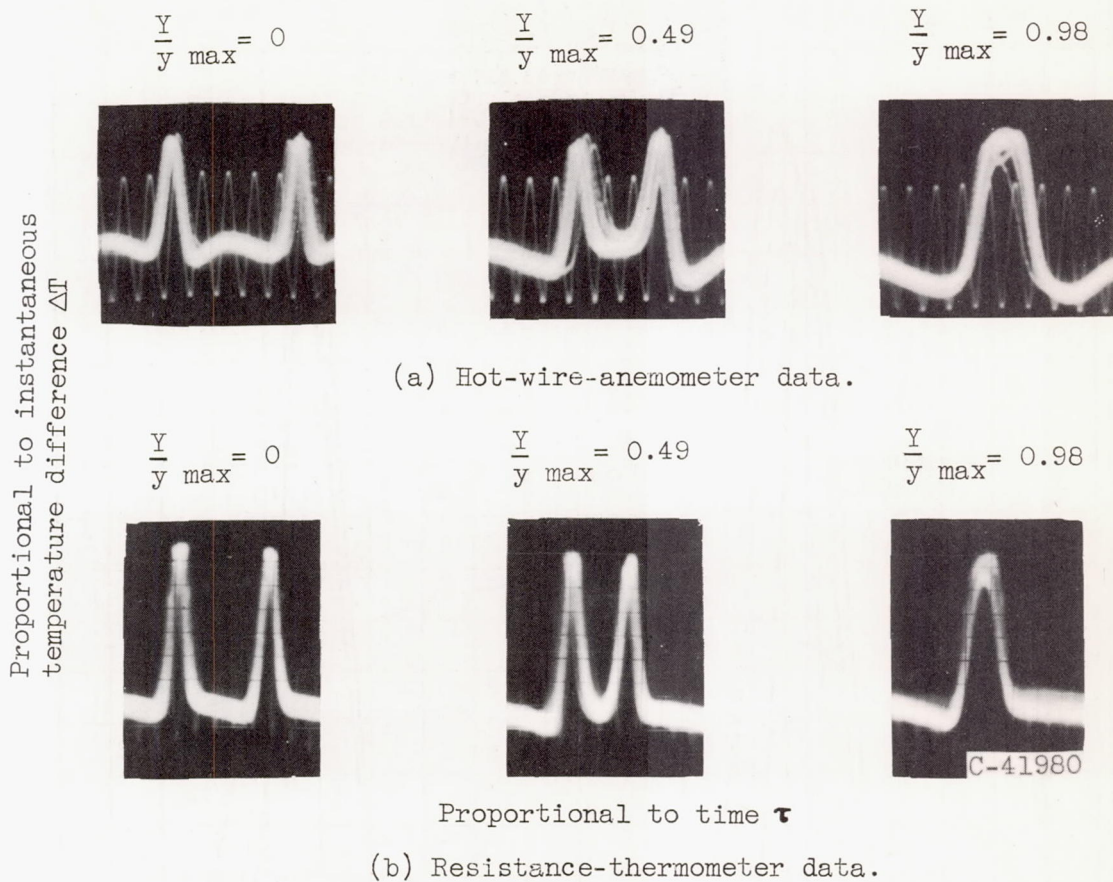
Figure 8. - Instantaneous-temperature-difference oscillograms. $X = 2.98$ inches or $\frac{fX}{U} = 1.47$.
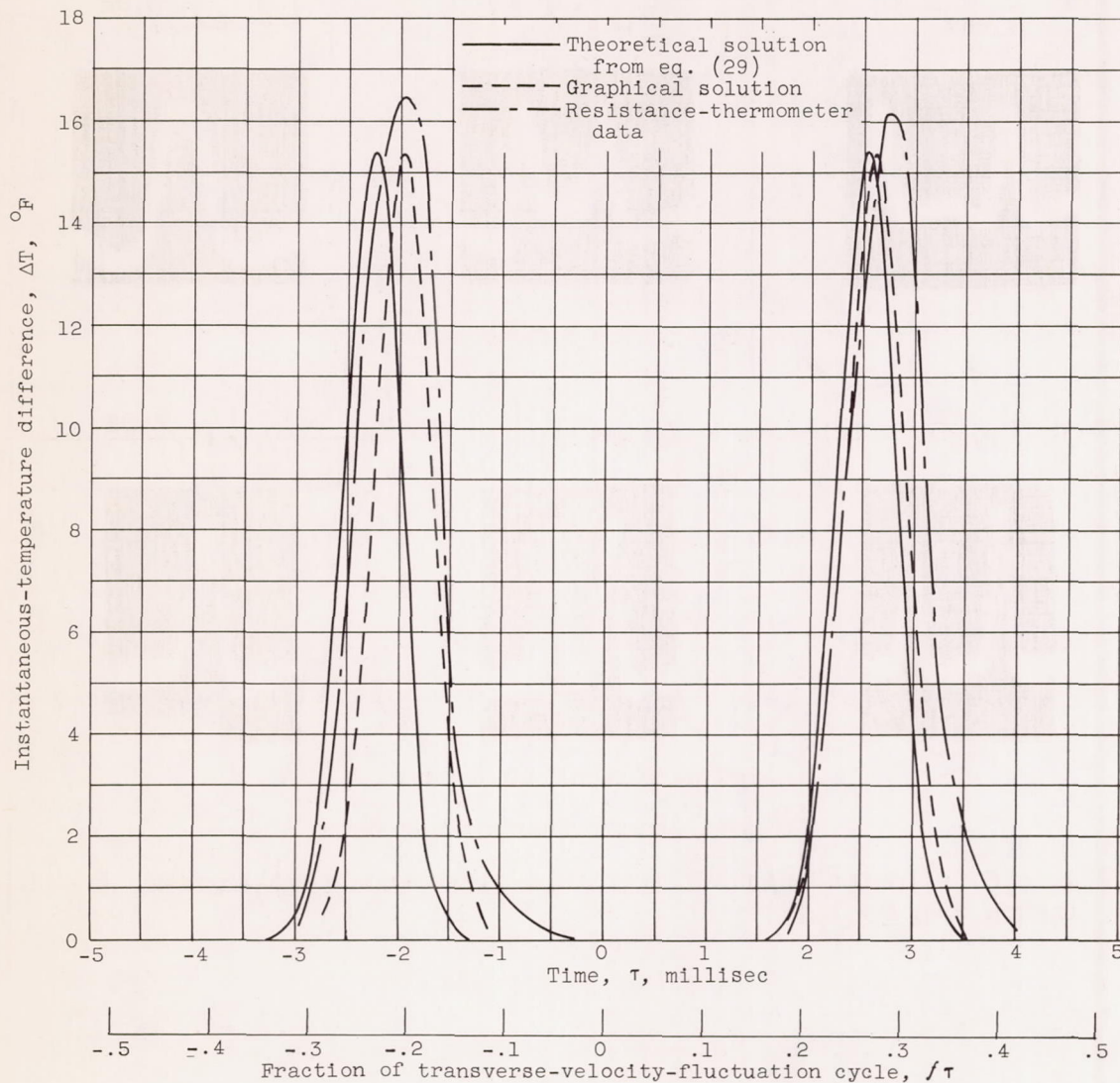
4022

(a) Lateral position, Y = 0 inch.

Figure 9. - Instantaneous temperature-time variation at various lateral positions.
X = 2.98 inches or fX/U = 1.47.
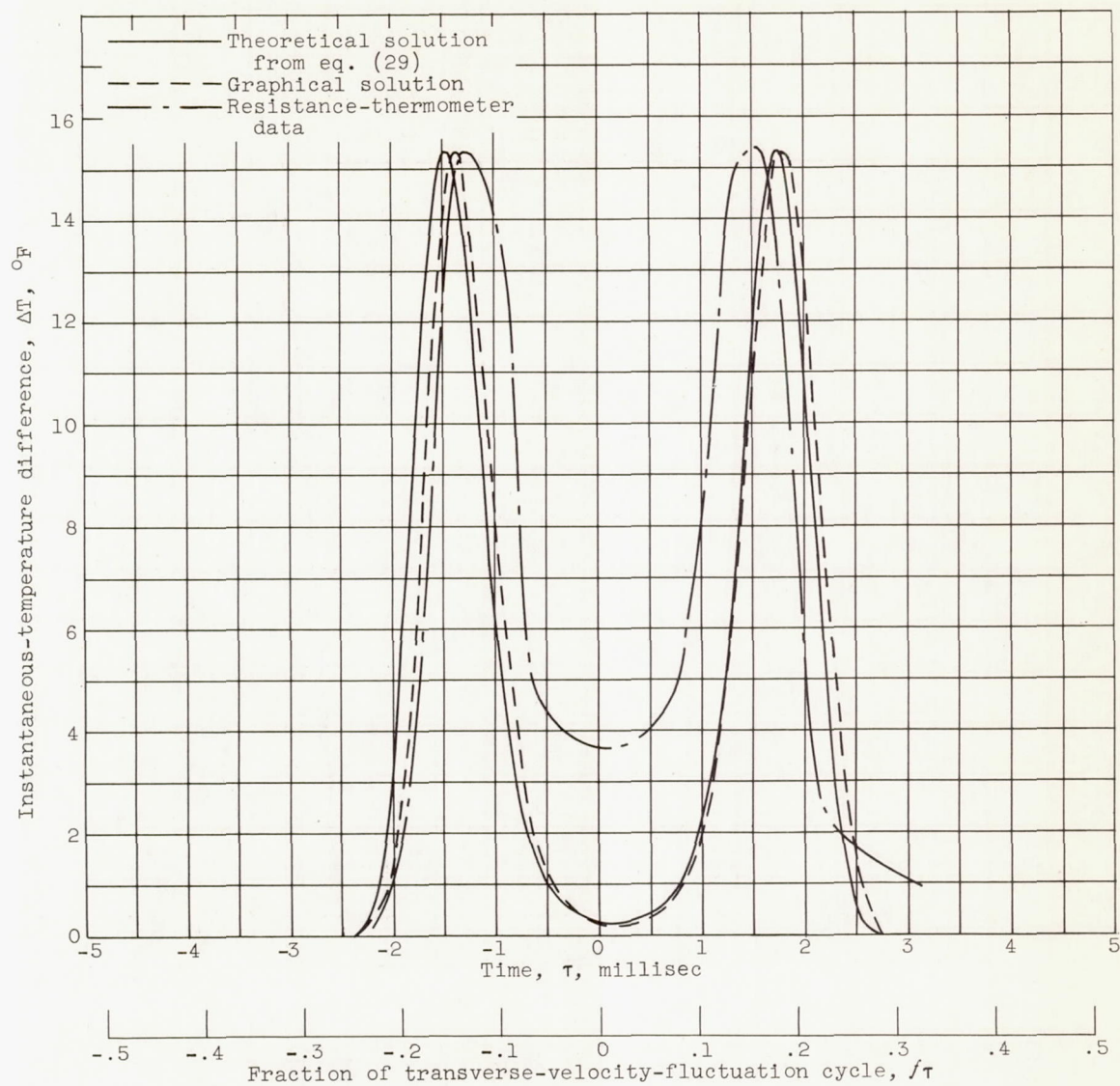
(b) Lateral position, Y = 0.085 inch or Y/y_{max} = 0.49.

Figure 9. - Continued. Instantaneous temperature-time variation at various lateral positions. X = 2.98 inches or fX/U = 1.47.

CL-9
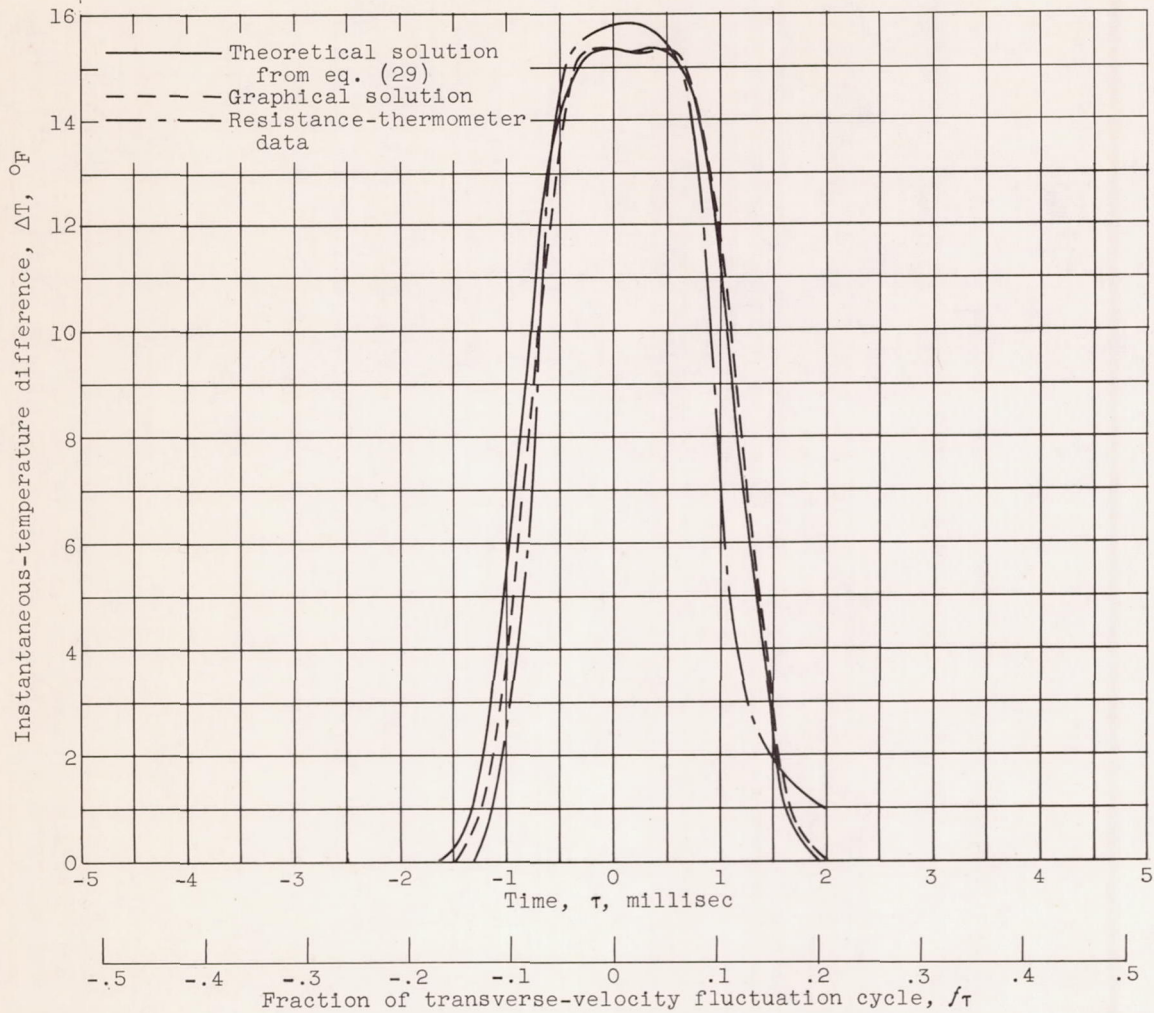
(c) Lateral position, $Y = 0.17$ inch or $Y/y_{max} = 0.98$.

Figure 9. - Concluded. Instantaneous temperature-time variation at various lateral positions. $X = 2.98$ inches or $fX/U = 1.47$.
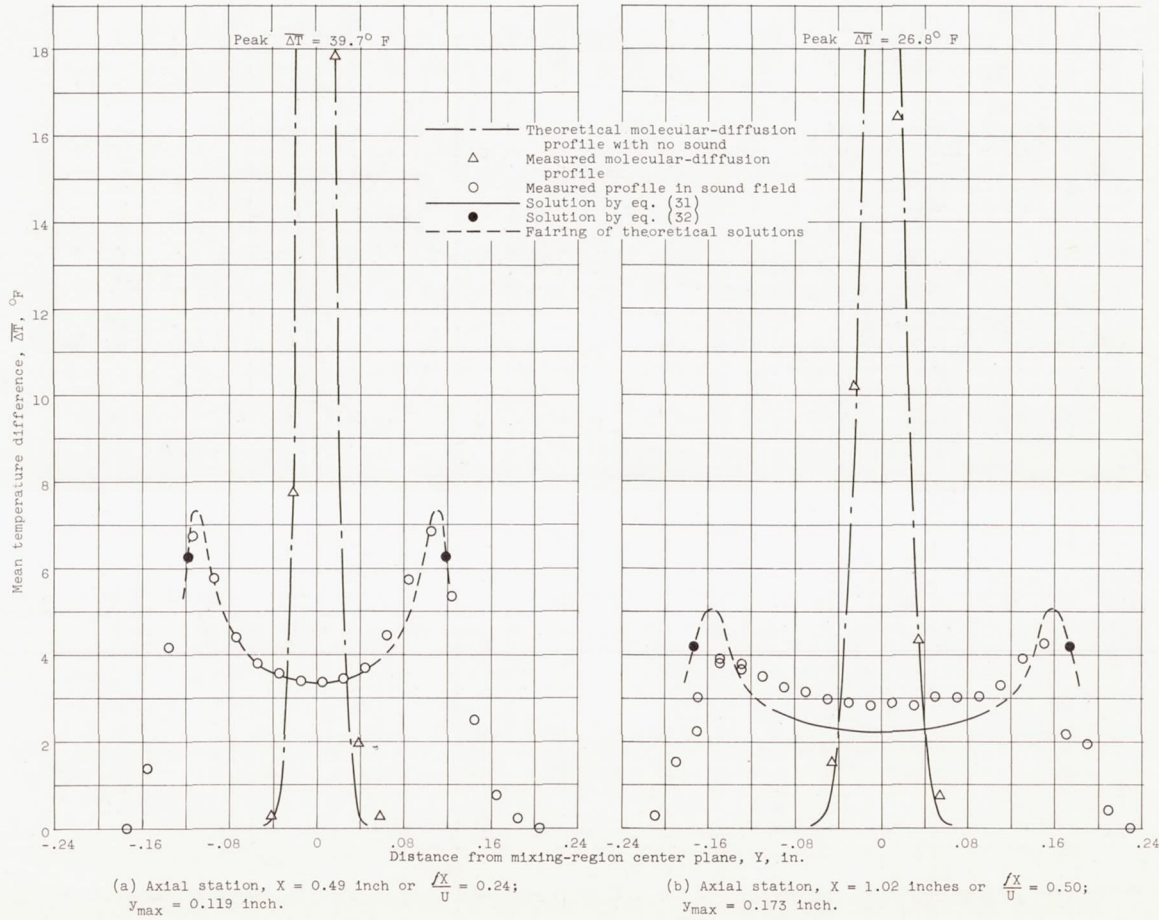
Figure 10. - Comparison of theoretical and experimental time-mean temperature-difference profiles at various axial stations.
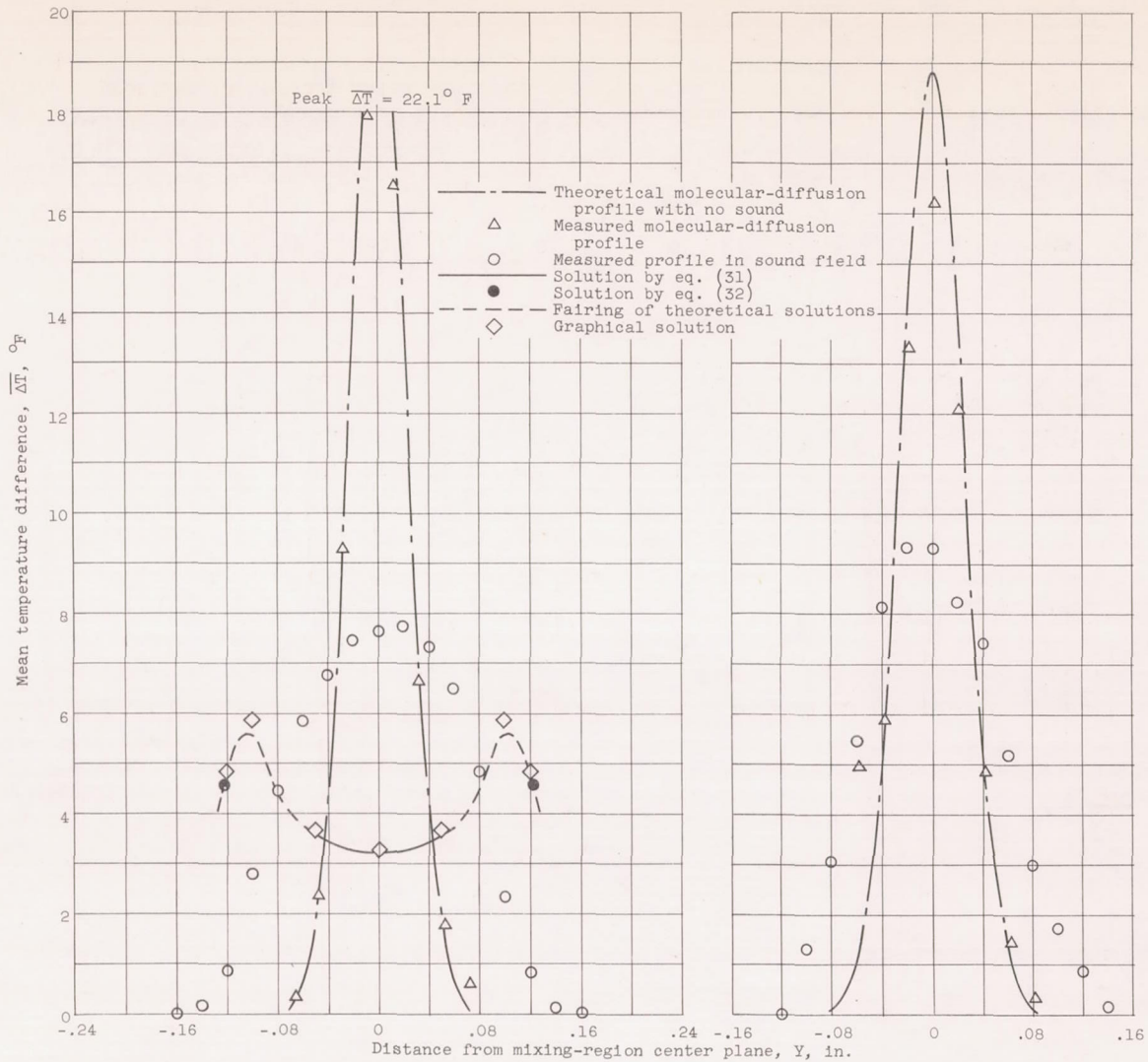
Peak $\overline{\Delta T} = 22.1^\circ$ F

Mean temperature difference, $\overline{\Delta T}$, $^\circ$F

Theoretical molecular-diffusion
  profile with no sound
△ Measured molecular-diffusion
  profile
○ Measured profile in sound field
—— Solution by eq. (31)
● Solution by eq. (32)
---- Fairing of theoretical solutions
◇ Graphical solution

−.24   −.16   −.08   0   .08   .16   .24   −.16   −.08   0   .08   .16

Distance from mixing-region center plane, Y, in.

(c) Axial station, X = 1.52 inches or $\dfrac{fX}{U}$ = 0.75;
  y_{max} = 0.123 inch.

(d) Axial station, X = 2.03 inches or
  $\dfrac{fX}{U}$ = 1.00.

Figure 10. - Continued. Comparison of theoretical and experimental time-mean temperature-difference
  profiles at various axial stations.
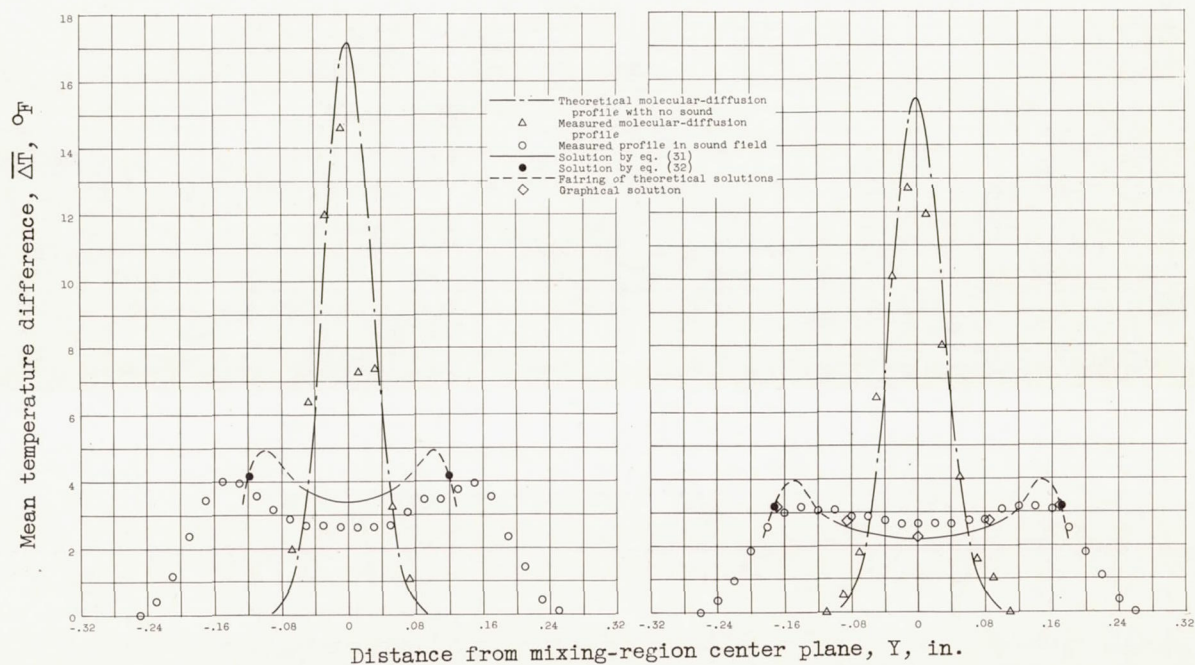
(e) Axial station, $X = 2.51$ inches or $\frac{fX}{U} = 1.24$; $y_{max} = 0.119$.

(f) Axial station, $X = 2.98$ inches or $\frac{fX}{U} = 1.47$; $y_{max} = 0.172$ inch.

Figure 10. - Continued. Comparison of theoretical and experimental time-mean temperature-difference profiles at various axial stations.
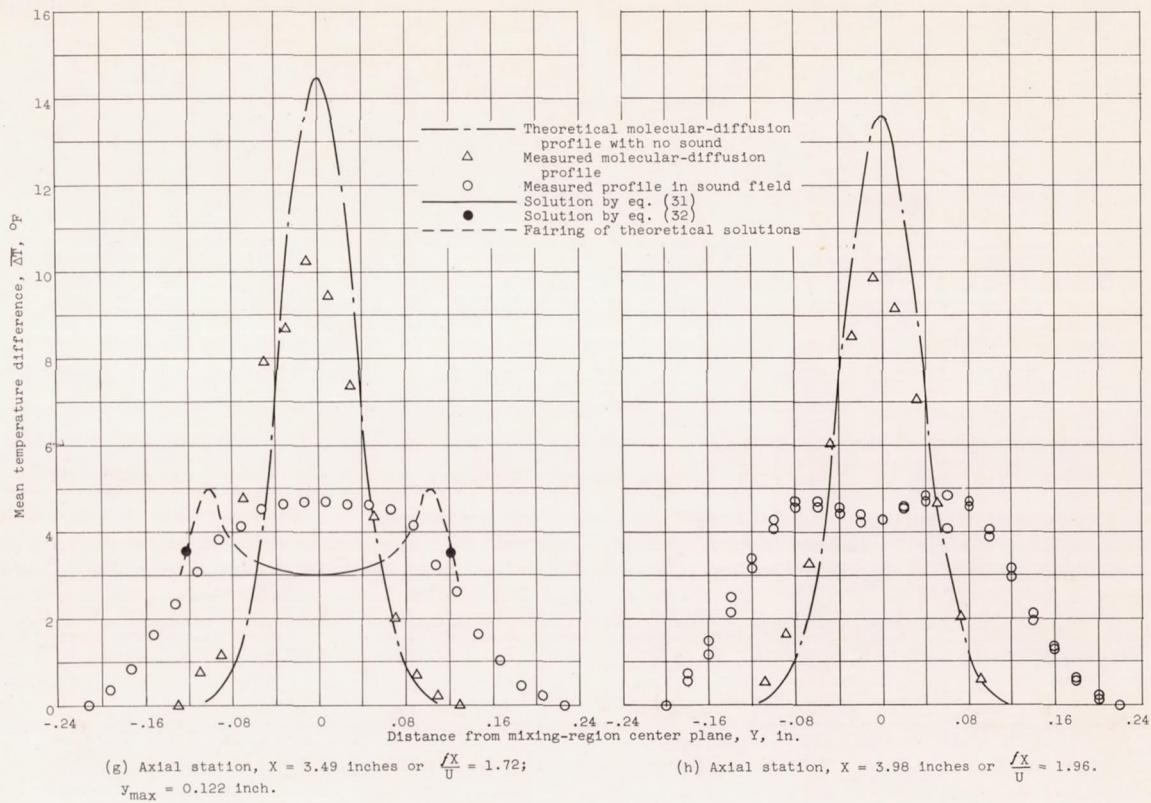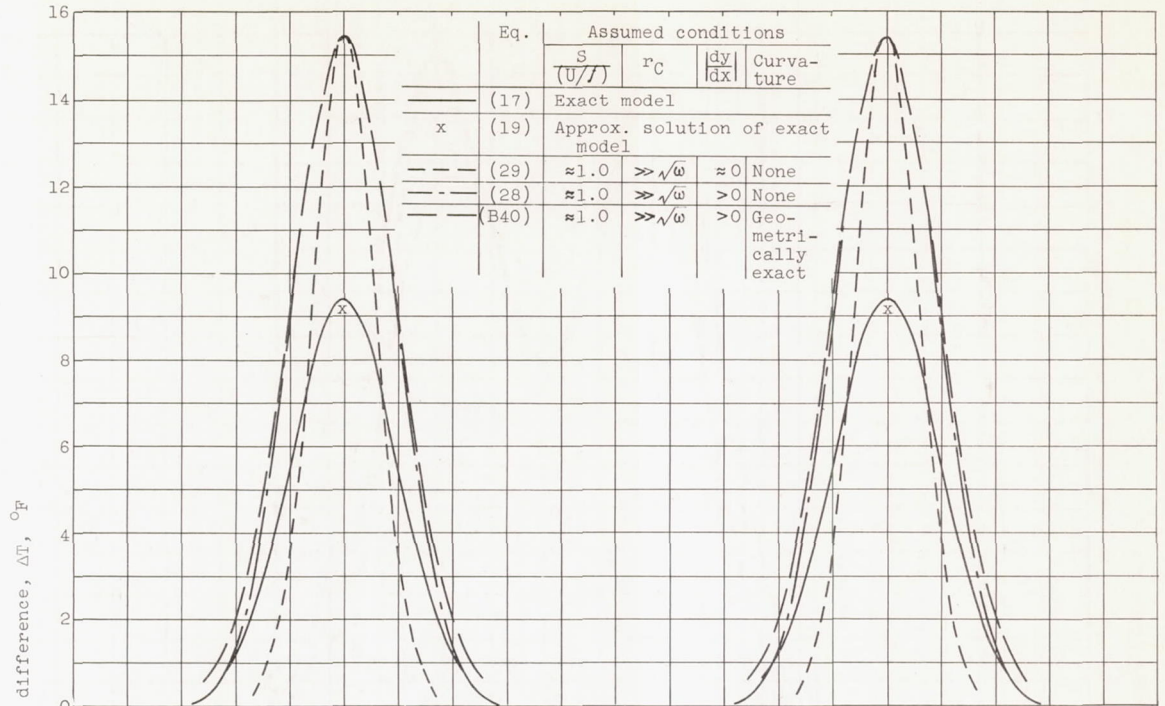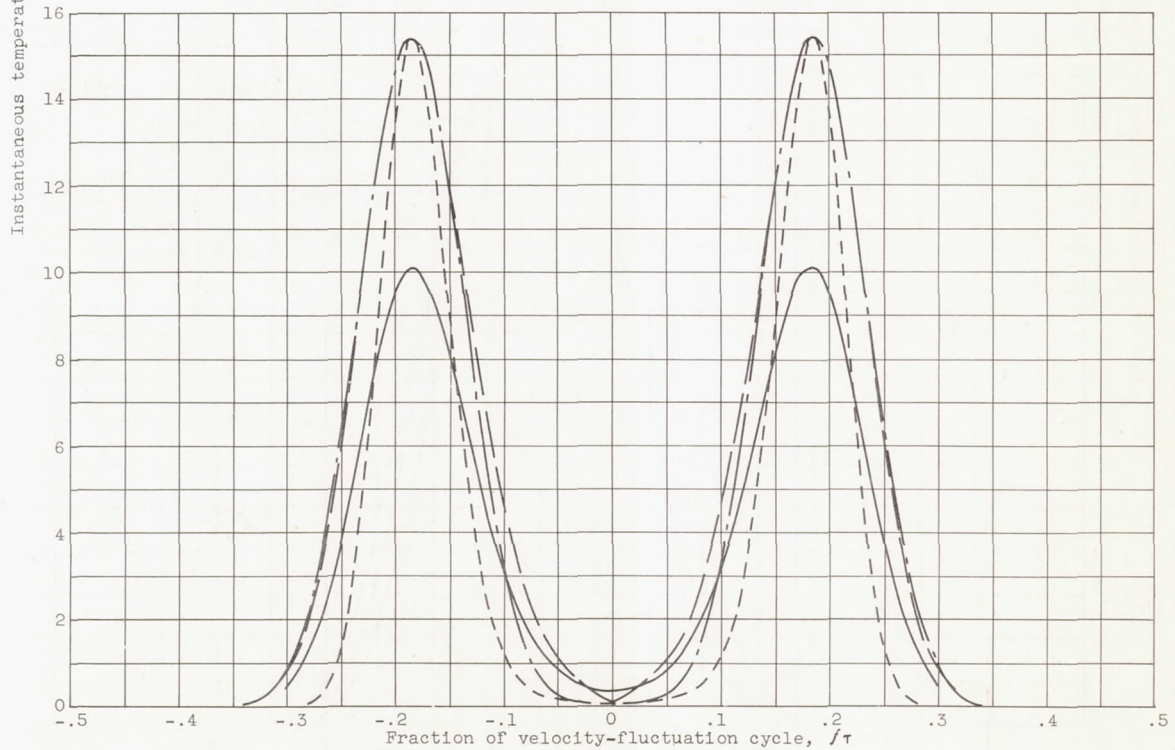
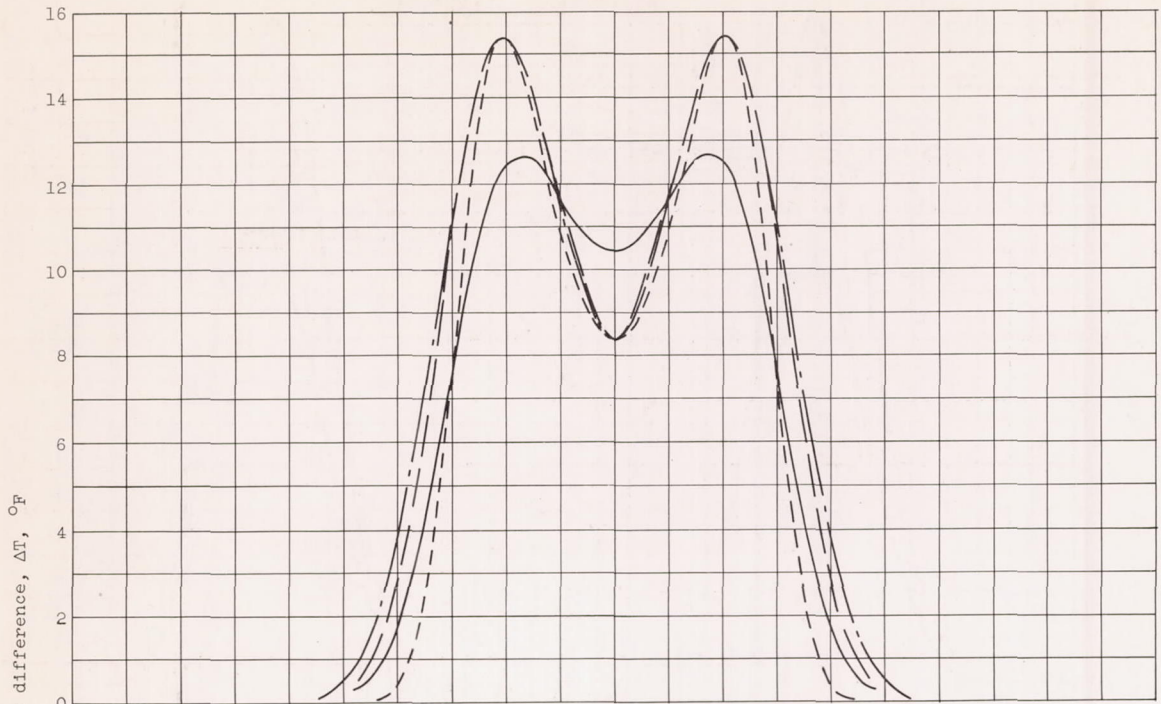(g) Axial station, X = 3.49 inches or $\frac{fX}{U}$ = 1.72; y_{max} = 0.122 inch.

(h) Axial station, X = 3.98 inches or $\frac{fX}{U}$ ≈ 1.96.

Figure 10. - Concluded. Comparison of theoretical and experimental time-mean temperature-difference profiles at various axial stations.

Eq.	Assumed conditions			
	$\frac{S}{(U/I)}$	r_C	$\left|\frac{dy}{dx}\right|$	Curvature
(17)	Exact model			
(19)	Approx. solution of exact model			
(29)	≈ 1.0	$\gg \sqrt{\omega}$	≈ 0	None
(28)	≈ 1.0	$\gg \sqrt{\omega}$	> 0	None
(B40)	≈ 1.0	$\gg \sqrt{\omega}$	> 0	Geometrically exact

(a) Temperature-time variation at $Y/y_{max} = 0$.

(b) Temperature-time variation at $Y/y_{max} = 0.4$.

Figure 11. - Comparison of exact and approximate solutions for instantaneous temperature. Dimensionless axial position, 7.5; coefficient of thermal diffusivity, 2.37×10^{-4} square feet per second; stream-velocity - frequency ratio, 0.0338 foot; ratio of root-mean-square velocity fluctuation to stream velocity, 0.947; rate of heat release from line source per unit length, 0.0308 Btu per second per foot.

(c) Temperature-time variation at $Y/y_{max} = 0.8$.

	Eq.	Assumed conditions			
		$\dfrac{S}{(U/f)}$	r_C	$\left|\dfrac{dy}{dx}\right|$	Curvature
——	(17)	Exact model			
x	(19)	Approx. solution of exact model			
– – –	(29)	≈ 1.0	$\gg \sqrt{\omega}$	≈ 0	None
– · –	(28)	≈ 1.0	$\gg \sqrt{\omega}$	> 0	None
— —	(B40)	≈ 1.0	$\gg \sqrt{\omega}$	> 0	Geometrically exact
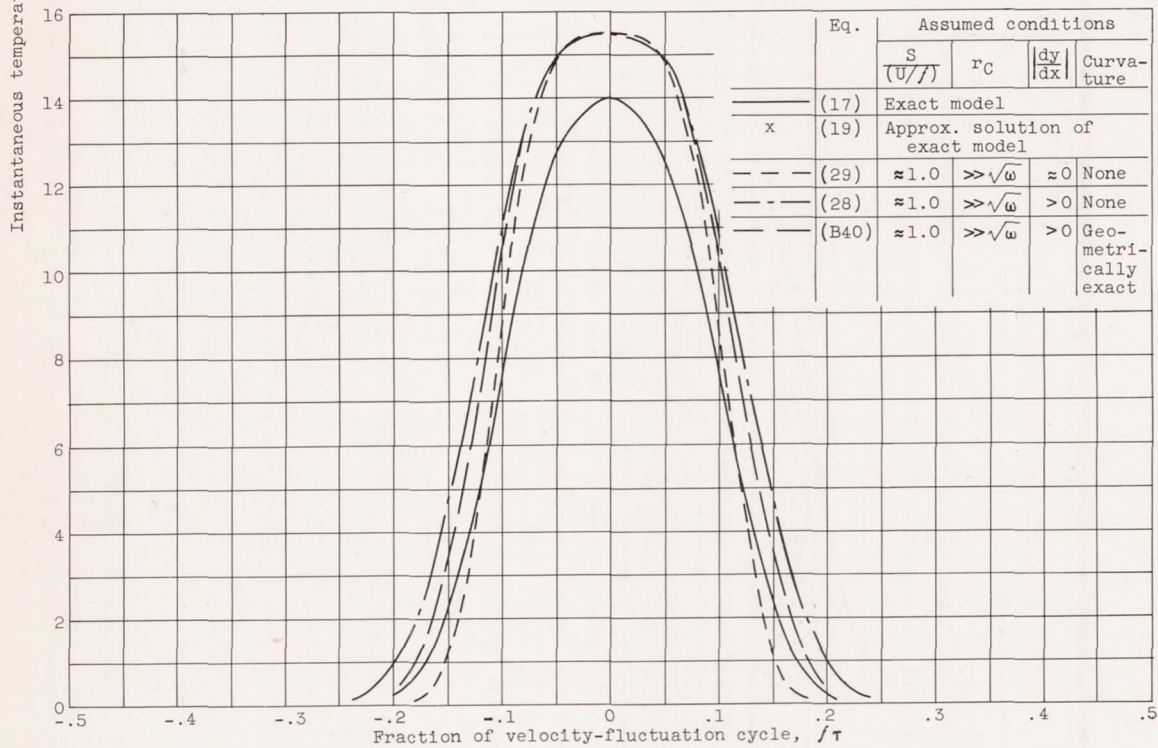
(d) Temperature-time variation at $Y/y_{max} = 1.0$.

Figure 11. - Concluded. Comparison of exact and approximate solutions for instantaneous temperature. Dimensionless axial position, 7.5; coefficient of thermal diffusivity, 2.37×10^{-4} square feet per second; stream-velocity - frequency ratio, 0.0338 foot; ratio of root-mean-square velocity fluctuation to stream velocity, 0.947; rate of heat release from line source per unit length, 0.0308 Btu per second per foot.
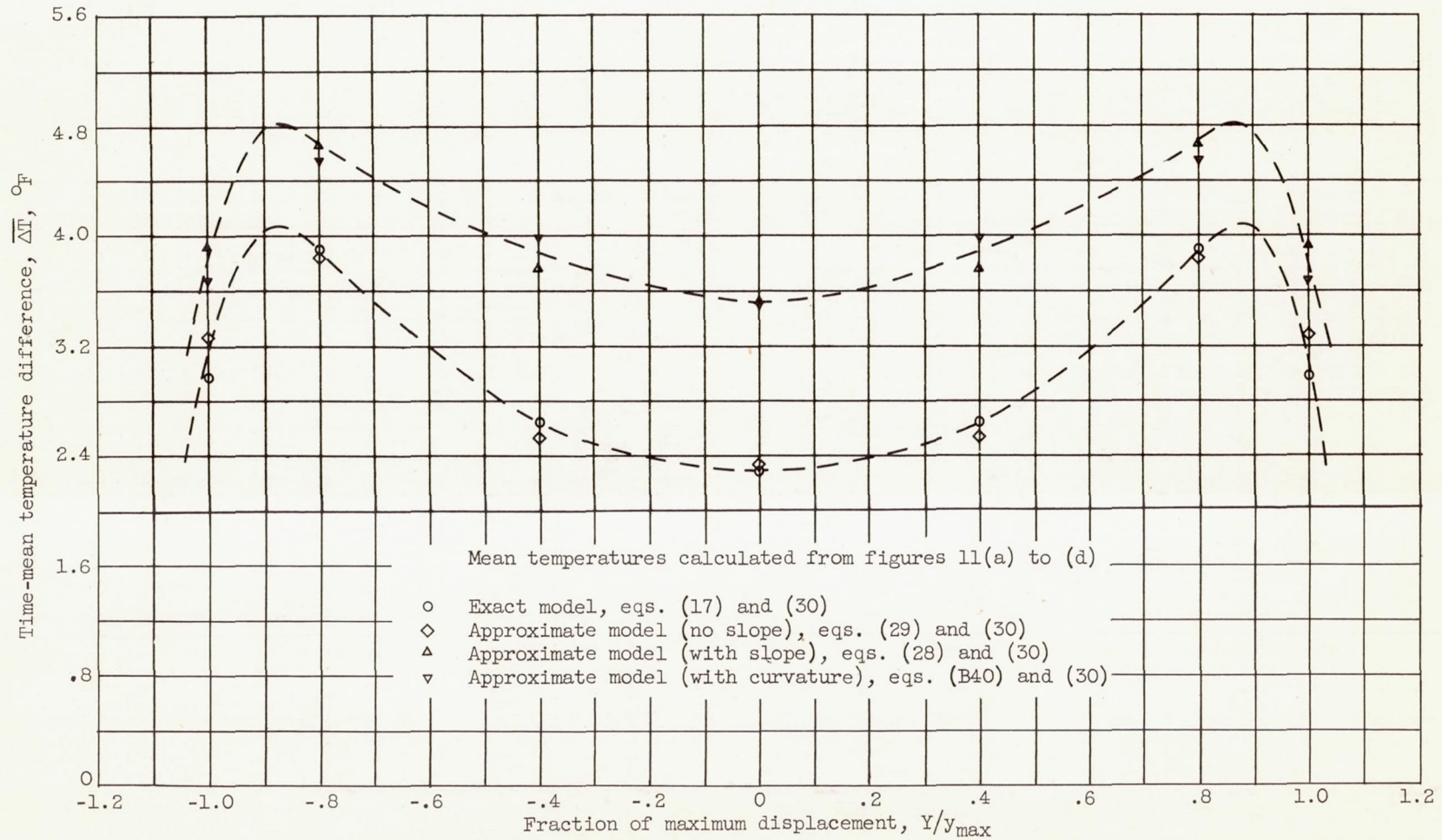
Figure 12. - Comparison of exact and approximate solutions for mean temperature. Dimensionless axial position, 7.5; coefficient of thermal diffusivity, 2.37×10^{-4} square feet per second; stream-velocity - frequency ratio, 0.0338 foot; ratio of root-mean-square velocity fluctuation to stream velocity, 0.947; rate of heat release from line source per unit length, 0.0308 Btu per second per foot.
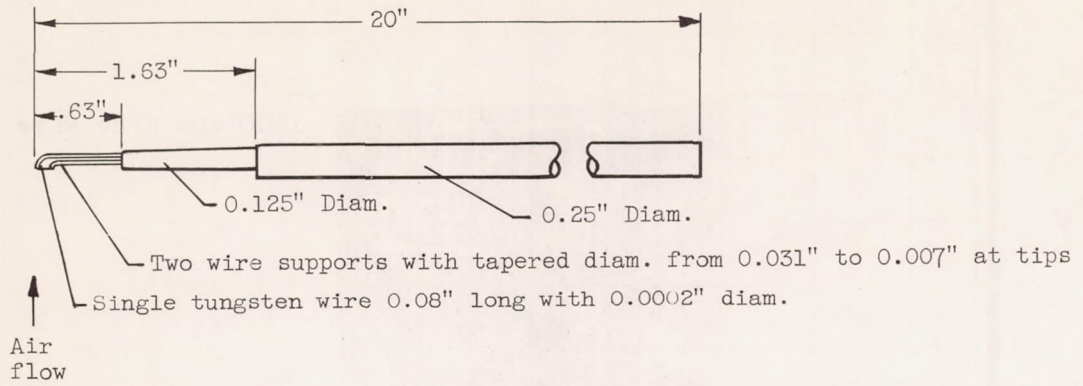
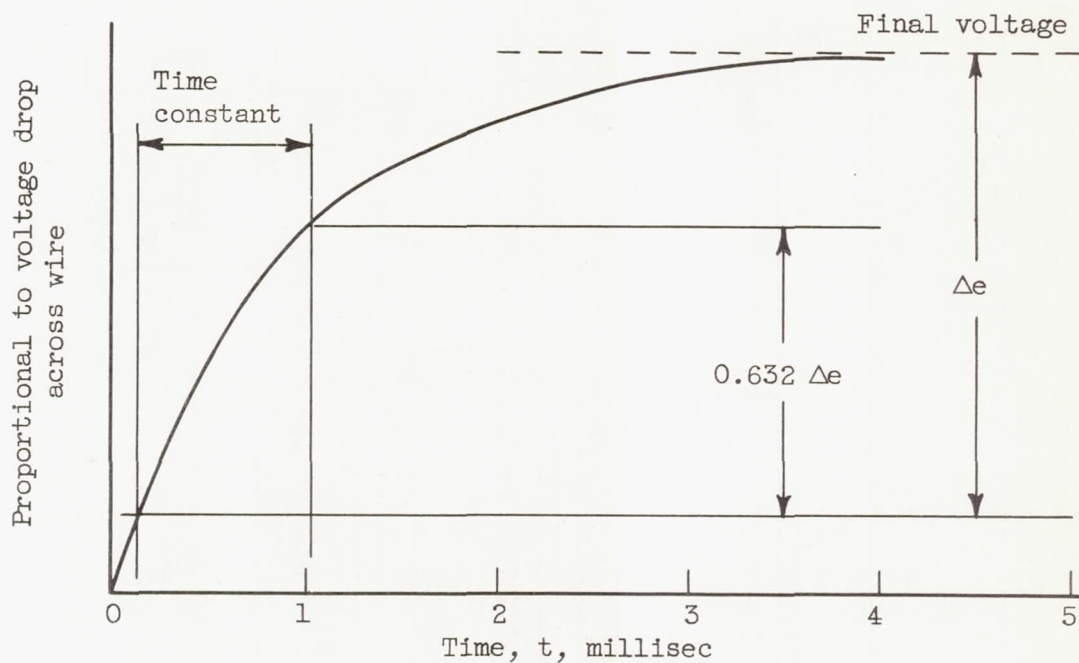(a) Resistance-thermometer probe.
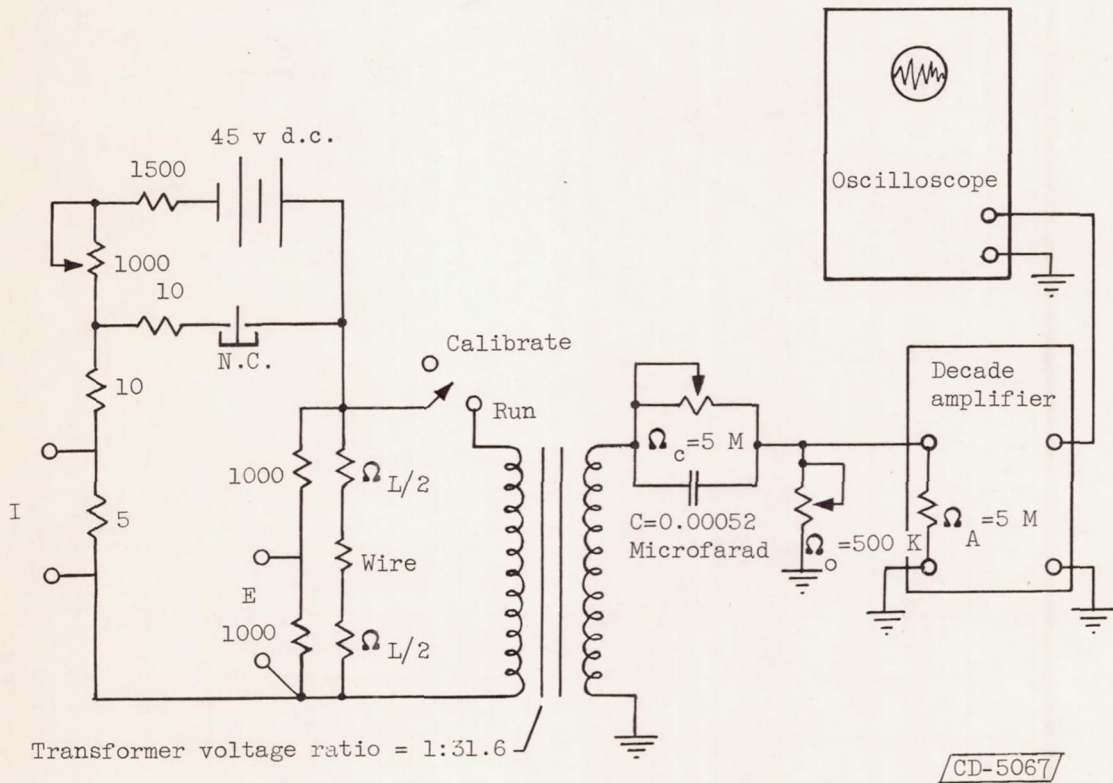
(b) Resistance-thermometer circuit.

Figure 13. - Resistance-thermometer instrumentation.

-1000 cps sine wave

C-42529
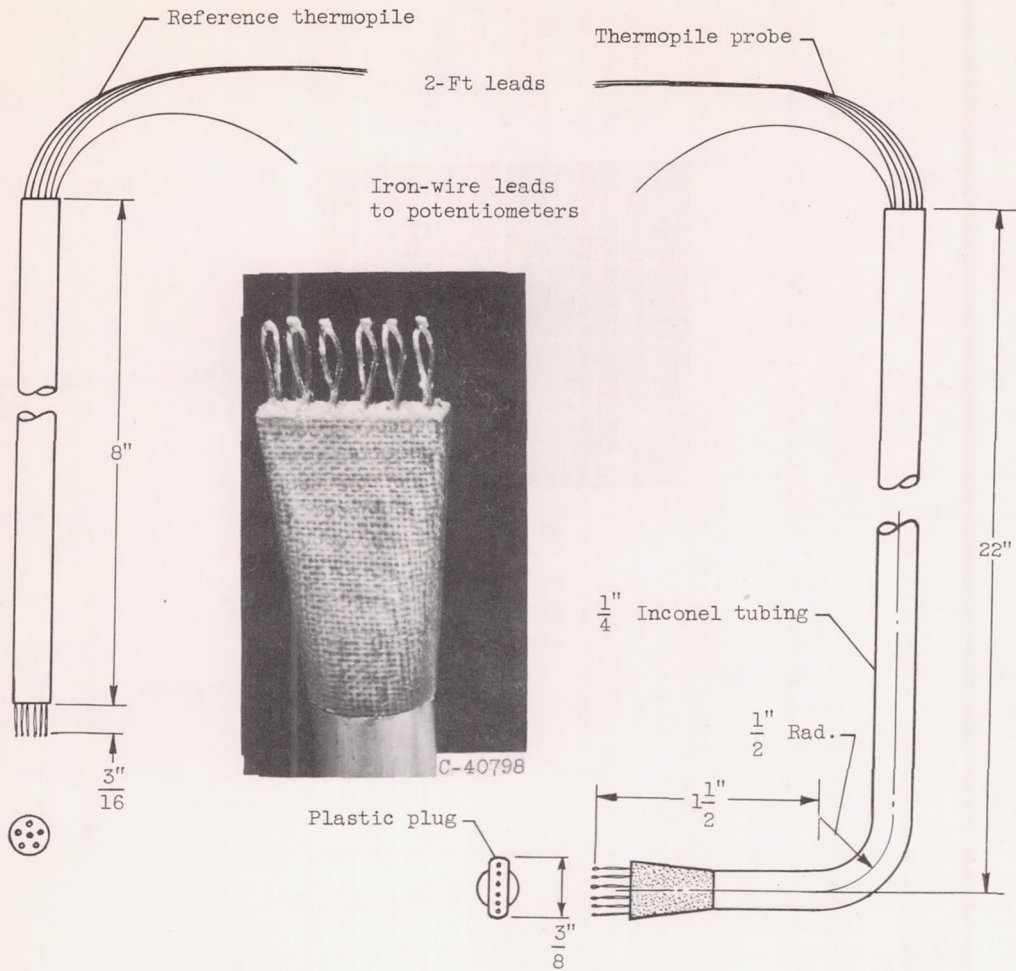
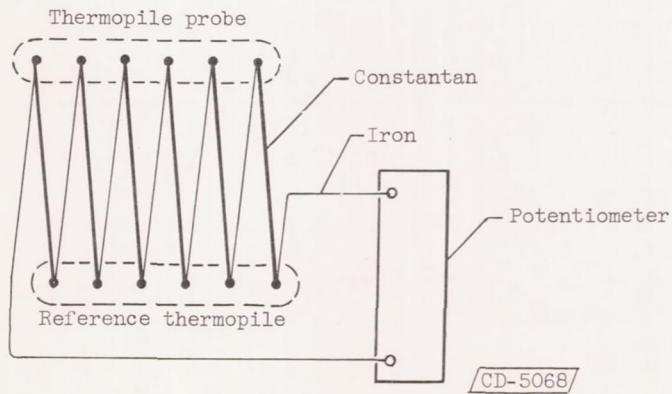- Wire response to step function current
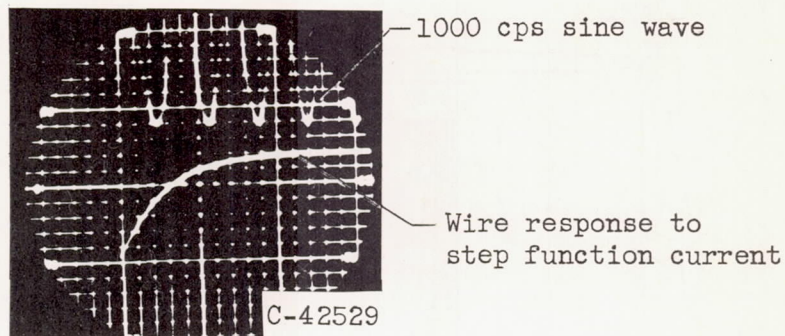
(a) Oscillogram

(b) Graphical construction.

Figure 14. - Determination of time constant of resistance-thermometer wire.

(a) Thermopile probe and reference thermopile.

(b) Thermopile circuit.

Figure 15. - Thermopile instrumentation.